JACS
JOURNAL OF THE AMERICAN CHEMICAL SOCIETY

Perspective

pubs.acs.org/JACS

Plasmonically Engineered Nanoprobes for Biomedical Applications

Amit Kumar, Sungi Kim, and Jwa-Min Nam*

Department of Chemistry, Seoul National University, Seoul 151-747, South Korea

ABSTRACT: The localized surface plasmon resonance of metal nanoparticles is the collective oscillation of electrons on particle surface, induced by incident light, and is a particle composition-, morphology-, and coupling-dependent property. Plasmonic engineering deals with highly precise formation of the targeted nanostructures with targeted plasmonic properties (e.g., electromagnetic field distribution and enhancement) via controlled synthetic, assembling, and atomic/molecular tuning strategies. These plasmonically engineered nanoprobes (PENs) have a variety of unique and beneficial physical, chemical, and biological properties, including optical signal enhancement, catalytic, and local temperature-tuning photothermal properties. In particular, for biomedical applications, there are many useful properties from PENs including LSPR-based sensing, surface-enhanced Raman scattering, metal-enhanced fluorescence, dark-field light-scattering, metal-mediated fluorescence resonance energy transfer, photothermal effect, photodynamic effect, photoacoustic effect, and plasmon-induced circular dichroism. These properties can be utilized for the development of new biotechnologies and biosensing, bioimaging, therapeutic, and theranostic applications in medicine. This Perspective introduces the concept of plasmonic engineering in designing and synthesizing PENs for biomedical applications, gives recent examples of biomedically functional PENs, and discusses the issues and future prospects of PENs for practical applications in bioscience, biotechnology, and medicine.

1. INTRODUCTION

Many metal nanoparticles (NPs), such as gold and silver NPs, possess promising properties such as high surface area, controllability of a variety of nanoscale structural features, and availability of conjugation sites on surface. More interestingly, these metal NPs can confine and amplify the light within an ultrasmall volume of a particle due to the localization and coupling of surface plasmons (collective oscillation of free electrons) with electromagnetic waves [this is called the localized surface plasmon resonance (LSPR)].[1] Augmented electromagnetic field near the surface of a metal NP modulates and promotes a variety of physicochemical processes and applications such as non-linear optics,[2] surface-enhanced vibrational spectroscopies,[3] photovoltaics,[4] metamaterials,[5] photothermal transduction,[6] plasmonic catalysis,[7] and "hot electron−hole" pair generation.[8] In particular, these NPs are quite useful for biomedical applications. In this regard, these particles provide strong, controllable optical properties, high controllability in composition and structure, availability of various synthetic schemes in forming targeted nanostructures in a high yield, reliable bioconjugation chemistries, implantability of multifunctionality in a single particle, high stability, and biocompatibility.[9] Among these, designing and tuning the plasmonic properties of these particles, including enhanced optical, photothermal, and photoacoustic properties, have been of special interest recently. However, precise engineering of these plasmonic properties on a nanometer scale and designing principles of these plasmonic bioprobes for the clinical applications are still ongoing subjects and under heavy scrutiny.[10]

The LSPR-dependent properties can be engineered based on the judicious selection of the size, shape, composition, and coupling of plasmonic NPs. The synthesis and proper use of such plasmonically engineered nanoprobes (PENs) based on the detailed, correct understanding of these probes for a specific biomedical application are key to successful development of plasmonic bioprobes (Figure 1A).[11] In deciding the plasmonic properties of PENs, nanoscale structural features such as junction, hollowness, sharp edge, pointed tip, flat interface, and symmetry along with strong plasmonic coupling-inducing plasmonic nanogap are critical and allow for controlling the plasmonic properties and augmenting the electromagnetic field of PENs.[12] Further, small organic molecules, surfactants, polymers, biomolecules such as DNA and proteins, and DNA origamis have been utilized to modulate and facilitate the formation of targeted PEN structures with targeted plasmonic features, and these cause crystallographic surface strain for lattice mismatch and different metal growth kinetics.[13] It should be noted that interparticle distances between plasmonic NPs or plasmonic gap size and shape largely affect the plasmonic properties of PENs. Controlling these distances on the nanometer or sub-nm scale is critical for tuning their optical and other plasmonic properties.[11] Another important part is the symmetry of nanostructures, and the symmetry breaking of PENs can generate higher electromagnetic field, multipolar plasmon modes, and new plasmonic properties such as Fano resonances and plasmon-induced transparency.[14] From the perspective of synthetic accessibility of many different PEN structures, the intrinsic crystallographic symmetry of NP seeds normally exhibits epitaxial symmetrical growth. However, playing with factors such as morphology, reducing agents, crystallographic mismatch, choice of the capping ligands, and control of kinetic and thermodynamic conditions can result in various non-spherical, asymmetric structures.[15,16] Further, biomolecule-mediated assemblies of PENs into chiral configurations give rise to the chiroplasmonic response that can be used as a highly sensitive and selective signaling tool for biodetection.[17,18] Also, the shift in chiroplasmonic absorption

Received: September 8, 2016
Published: October 10, 2016

DOI: 10.1021/jacs.6b09451
J. Am. Chem. Soc. 2016, 138, 14509−14525

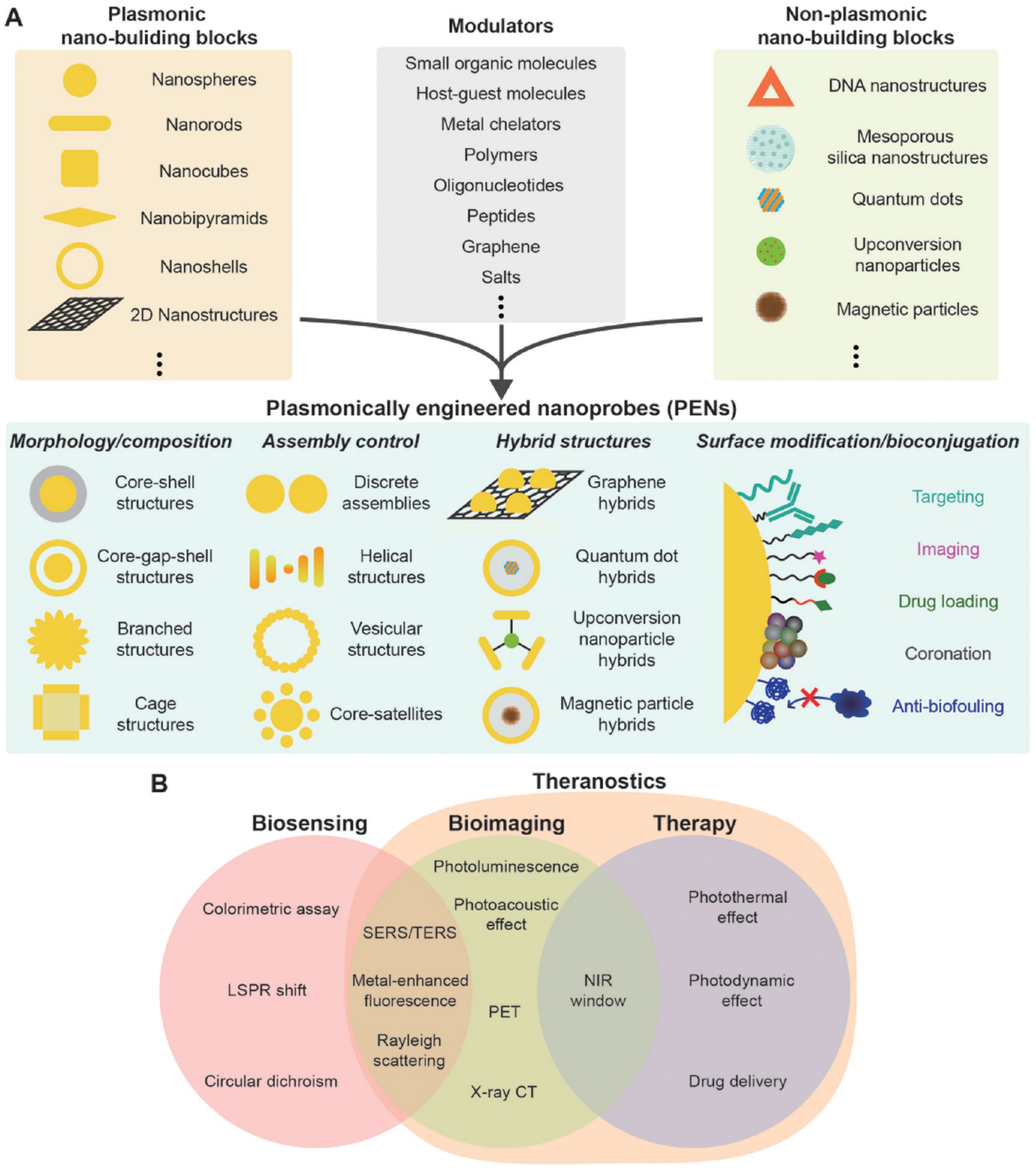

Figure 1. Plasmonically engineered nanoprobes (PENs) for biomedical applications. (A) Tuning and combining plasmonic building blocks, non-plasmonic building blocks, and modulators and formation of PENs via engineering particle morphology, particle composition, assembled structure, hybrid structure, surface modification, and bioconjugation. (B) Representative biomedical applications of PENs.

wavelength upon interaction with chiral biomolecules such as proteins gives secondary and tertiary structural information.[19]

Designing and integrating nanoprobes with plasmon-induced beneficial features for biomedical applications is a challenging task due the complexity in structure design and synthesis and understanding of the properties for a variety of applications under different *in vitro* and *in vivo* environments in bioscience and medicine (Figure 1).[20,21] Further, clinical studies and eventual use in medicine are time- and money-consuming and highly complicated due to the complex physiologies and a myriad of different needs and issues that should be fully addressed for each case. To achieve this challenging goal, designing, synthesizing, and validating PENs for a specific application are of foremost importance. In this Perspective, we provide basic concepts of PENs for biomedical applications and review and discuss recent advances, issues, and future directions of this field.

DOI: 10.1021/jacs.6b09451
J. Am. Chem. Soc. 2016, 138, 14509−14525

2. DESIGN AND SYNTHETIC STRATEGIES OF PLASMONICALLY ENGINEERED NANOPROBES

In general, the plasmonic engineering of nanostructures is based on and can be built with plasmonic and non-plasmonic building blocks and structure- and function-controllable modulators for eventual formation of PENs with targeted structure and functionality (Figure 1A). The plasmonic properties of these nanostructures can be designed, predicted, and analyzed by applying fitting computer simulation techniques. Modulators can tune the plasmonic structural details such as plasmonic coupling and facilitate complex plasmonic structures (Figure 1A, bottom). The position and the number of dye molecules (e.g., Raman and fluorescent dyes) can be also modified to and controlled by modulators. Non-plamonic building blocks can be used as templates for introducing molecular and nanostructural moieties in a controlled manner and add other multi-functionalities including magnetic and upconversion properties and porosity. For biomedical applications of these PENs, it is critical to functionalize them by proper, reliable bioconjugation and surface modification chemistries (Figure 1A, bottom right). The optical properties of plasmonic NPs are primarily engineered by tuning their size, shape, chemical composition, and dielectric environment.[22,23] The plasmonic properties of metal NPs can essentially be described using classical electrodynamic Mie theory.[24−26] The extinction cross section (C_{ext}) for a metal nanosphere can be represented as

$$C_{ext}(\omega, R) = 12\pi \frac{\omega R^3 \varepsilon_m^{3/2}}{c} \frac{\varepsilon_2(\omega, R)}{[\varepsilon_1(\omega, R) + 2\varepsilon_m]^2 + \varepsilon_1(\omega, R)^2}$$

where R is the radius, c is the speed of light, ε_m is the dielectric constant of the surrounding medium, ω is the frequency, and $\varepsilon(\omega,R) = \varepsilon_1(\omega,R) + i\varepsilon_2(\omega,R)$; $\varepsilon_1(\omega,R)$ and $i\varepsilon_2(\omega,R)$ are the real and complex parts of the material dielectric constant, respectively. Based on this equation, the extinction properties of spherical plasmonic NPs can be tuned by altering the size and dielectric properties of the material and medium/environment. In contrast, anisotropic NPs can support multiple plasmon modes, depending on the complexity of the nanostructure.[27,28] In general, the number of plasmon resonant frequencies depends on the number of polarizable ways of a nanostructure. Various numerical modeling methods, such as discrete dipole approximation,[29] T-matrix,[30] finite-difference time domain,[31] finite-element modeling,[32] and the boundary element method,[33] have been developed to study NP plasmonics. Overall, a red shift and increase in resonance peak intensity occurs when spherical NP size is increased. Upon increasing the corner sharpness and extent of anisotropy, there is a red-shift in the resonant frequency for anisotropic nanostructures. Separation of charge with mirror symmetry also increases the intensity of the resonant peak. These basic principles of plasmonic engineering have been applied to design the plasmonic nanostructures and optimize the desired optical response of plasmonic NPs such as gold nanorods (AuNRs),[34] gold nanoshells (AuNSs),[35] gold nanocages,[36] and branched nanostructures (Figure 1).[37]

Well-defined assemblies of plasmonic NPs where individual nanostructures such as spherical NPs and AuNRs are grouped in particular orientations and with definite interparticle distances are more challenging and have a larger scope and usage in a variety of applications, including biosensing and bioimaging (Figure 1A,B).[38] Typically, the close assembly of NPs where interparticle spacing is less than 2.5 times the particle diameter causes plasmonic coupling.[39,40] Generating and controlling a nanogap between two NP units in PEN assemblies is crucial for harnessing ultra-strong electromagnetic field through plasmonic coupling. For this purpose, DNA,[41] bifunctional organic ligands,[42] streptavidin−biotin conjugate,[43] thin layer of polymer,[44] silica coating,[45] and single-layered graphene[46] have been used as nanoscale molecular separators. Plasmonic coupling between metallic nanostructures can be understood by the analogy of atomic orbital coupling leading to molecular orbitals.[47] This plasmon hybridization model can be used to simulate complex nanostructures by theoretically disintegrating them into simple constituent structures and hybridizing the plasmon modes of each geometry. The optical properties of multimeric systems can also be influenced by the symmetries and orientations of individual NPs.[48,49] A periodic chart of plasmonic NPs can be designated as "plasmonic atoms" in different rows and columns, taking their shapes and geometrical parameters into account.[11,50] The assembly of such plasmonic atoms results in the formation of organized nanostructures (plasmonic molecules) under energetically favorable conditions, with the effect of directing agents/templates and/or by externally applying other stimuli such as forces (electrostatic, magnetic, flow, etc.).[13,51] This assembly can be applied to build, tune, and alter the nanostructures and their corresponding plasmonic properties.

For biomedical applications of PENs, particle surface modification and bioconjugation chemistry should be considered (Figure 1A). Understanding and engineering organic corona around plasmonic NPs is critical for providing the desired functionalities on the surface for various PENs and eventual *in vivo* fate of PENs. The structural features of stabilizing organic ligands on metal NPs play very important roles in their directed assembly and particle stability, and specific intermolecular interactions such as hydrogen bonding and electrostatic interactions among organic ligands affect aggregation, self-assembly, and targeting of PENs. Metal NP building blocks resulting from site-selective functionalization with a desired number of organic ligands on particle surface are profoundly useful for making targeted PENs accessible in a high yield.[52]

Highly designable and tunable biomolecules can be used as synthetic modulators and templates for PENs. Among them, single-stranded DNA (ssDNA) has been extensively used as ligands for well-defined and controllable 1D, 2D, and 3D plasmonic assemblies because ssDNA enables tuning of the number of DNA strands on each metal NP building block, base sequence, length/structure of oligonucleotides, and modification of functional moieties such as thiol and fluorophore.[53−55] DNA molecules can serve as programmable ligands to fine-tune the morphologies of nanomaterials depending on the shape of the seed and sequence of DNA used.[56−58] DNA molecules were found to play important roles by influencing diffusion of the Au precursor to the seed and modulating the growth through differences in DNA desorption, density, and mobility on the seed surface. It was also reported that sequence-controlled binding of thiolated DNA to a AuNP surface can facilitate the formation of an interior nanogap while forming Au shells on DNA-modified AuNPs.[59] Thiolated DNA-modified AuNPs have also been used to form Au−Ag head−body nano-snowman structures.[60] The nanojunction between Au head and Ag body can be finely tuned by varying the salt conditions and amount of Ag precursor, respectively. It was also shown that DNA strands can self-assemble into a stiff "nanomold" that contains a user-specified 3D cavity and encloses a nucleating gold "seed".[61] Under mild conditions, this seed grows into a larger cast structure that fills

DOI: 10.1021/jacs.6b09451
J. Am. Chem. Soc. 2016, 138, 14509−14525

and thus replicates the cavity, resulting in a metallic nanostructure of chosen shape and size. Another more intuitive method for constructing PENs is to assemble isolated plasmonic NPs (plasmonic atoms) into well-defined discrete assemblies (plasmonic molecules) with close interparticle distances in specific configurations. DNA serves as an ideal connector or bond between plasmonic atoms for such assemblies because of its highly specific and controllable molecular recognition capability and controllable length.[11,41,62] Further, advancements in DNA nanotechnology have resulted in the generation of a variety of DNA superstructures solely from DNA, utilizing the DNA tiles and DNA origamis, and these DNA nanostructures can act as "template networks" for the well-defined assembly of metal NPs.[62−64] Recently, specifically designed 2D DNA origami has been utilized to develop a precise and removable templating platform that can transfer 2D oligonucleotide patterns onto the surface of AuNPs through an engineered toehold-initiated DNA displacement reaction.[65] This strategy can be used to precisely control the number of valence and valence angles of AuNPs, and, further, these DNA-decorated AuNPs act as precursors for the construction of discrete AuNP clusters with desired configurations. Assembling plasmonic NPs into stereospecific 3D chiral configurations has wide applications in developing new classes of metamaterials and advanced biosensing platforms for chiral biomolecules. Recently, a 2D DNA origami template with an "X" arrangement of DNA capturing strands on both sides was utilized to assemble AuNRs into left-handed and right-handed AuNR helices.[66] Toroidal-shape chiral metamolecules, constructed from origami and spherical plasmonic NPs, showed strong chiroptical properties.[67] A walking plasmonic AuNR was demonstrated on DNA origami as an active plasmonic system, in which AuNR with DNA strand feet can execute directional, progressive, and reverse nanoscale walking on a 2D or 3D DNA origami platform.[68,69] This plasmonic system may be useful for imaging dynamic biological phenomenon that is involved with controlled motion at nanometer scale, which is well below the optical diffraction limit. DNA aptamers can also act as targeting moieties that can specifically bind to one type of cell.[70] More complex biomolecules such as peptides and their self-assembled supramolecular structures exhibit a wide range of functional groups and, depending on their amino acid sequences, can be used to both synthesize and assemble isotropic and anisotropic metal nanostructures in a controllable manner.[71−76] Recently, peptides of different chiralities have been used to artificially create chiroplasmonic responses in AuNPs through peptide−NP interactions.[77,78]

Due to strong, controllable plasmonic coupling and large light absorption and light-scattering cross section, PENs have been utilized as intense signal-generating labels for immunoassays, biochemical plasmonic sensors, and surface-enhanced Raman scattering (SERS) tags.[79,80] Biomolecule-mediated structural modification, assembly/disassembly, or change in dielectric environment of PENs can cause shift in LSPR absorption wavelength, and such label-free LSPR-based assays can be readily utilized for biosensing applications. Distance-dependent plasmonic coupling between metal nanostructures and the corresponding change in light-scattering properties has been exploited for characterizing and imaging biochemical processes, biomolecular interactions, and specific bioreceptor expressions.[43] Highly sensitive SERS biosensing schemes require an ultra-small interparticle nanogap (∼1 nm) in PENs as an electromagnetic hot-spot; slight deviation in hot-spot geometry and/or location of Raman reporter molecule causes tremendous fluctuations in Raman signals.[81] Therefore, plasmonic engineering of such SERS probes with suitable design and synthetic principles is crucial for signal reproducibility and single-molecule detection capability. Suitable positioning of fluorophore molecules with respect to the plasmonic NP surface can modulate the fluorescence signals in such a way that fluorescence signal enhancement is maximized while fluorescence signal quenching is minimized, and these metal-enhanced fluorescence (MEF) probes can be readily used for a variety of biosensing and bioimaging applications.[82]

Certain PENs with branching or hollow structural features can exhibit LSPR-induced thermoelastic expansion with generation of photoacoustic (PA) waves upon light irradiation at LSPR wavelength, and detection of such PA waves can be used for bioimaging applications.[83] For non-invasive cancer bioimaging applications, integrating multiple imaging modalities such as SERS, PA tomography (PAT), and computed tomography (CT) in a single probe possess remarkable advantages in terms of imaging sensitivity, high spatial resolution, and reliable tumor site identification.[84] Such multimodal bioimaging PENs have huge potential for clinical applications. PENs can also be designed for near-infrared (NIR) light-mediated photothermal transduction with well-controlled light-to-heat conversion efficiency, depending on the plasmonic structural features. It should be noted NIR light has several advantages for biomedical applications, including minimal interfering absorption and fluorescence from biosamples, relatively little scattering, deep tissue penetration, and low cost in laser diode excitation (Figure 1B). And, such PENs are potential candidates for non-invasive photothermal therapy (PTT) of deeply embedded malignant tumors.[85] Generation of hot electrons/holes in PENs in combination with plasmon-induced photocatalysis can convert normal oxygen to cytotoxic singlet oxygen, and such PENs have been tried for photodynamic therapy (PDT) of cancer as the alternate of conventional organic photosensitizers.[86] PENs having both therapeutic features, PTT and PDT, can be highly efficient for carrying out therapy at benign tissue temperature with minimized necrotic damage to the healthy cells.[87] Photothermal effect-induced release of therapeutic agent (drug or biomolecules) at a tumor site has been extensively studied using a variety of PEN structures, where PEN not only acts as efficient delivery vehicle but also delivers the cargo at target site using light-exposure as remote control.[88,89] Owing to the multifunctional features of PENs for bioimaging and PTT/PDT therapeutic properties, PENs offer excellent platforms for imaging-guided therapy or theranostics. With real-time imaging functionality during simultaneous therapeutic procedures, tumor sites are treated efficiently with high spatiotemporal precision.[90]

For biomedical applications of PENs, one should always notice that it is critical to have a highly specific binding capability for targets of interest with low non-specific binding to random objects. The properties of PENs should fit with biological environments (e.g., the use of NIR light is beneficial for its deep tissue penetration depth for imaging, activation of the plasmonic properties of NPs, and minimal non-specific bindings). Another important aspect is biocompatibility and low toxicity. For cells, cytotoxicity measurement is mainly done; however, for *in vivo* applications, along with cytotoxicity, the biodistribution of NPs inside bodies and excretion and accumulation of NPs should be also considered. *In vivo* particle stability and further modification of NPs to form coronas on particles can seriously affect the fate of NPs inside bodies.[91]

DOI: 10.1021/jacs.6b09451
J. Am. Chem. Soc. 2016, 138, 14509−14525

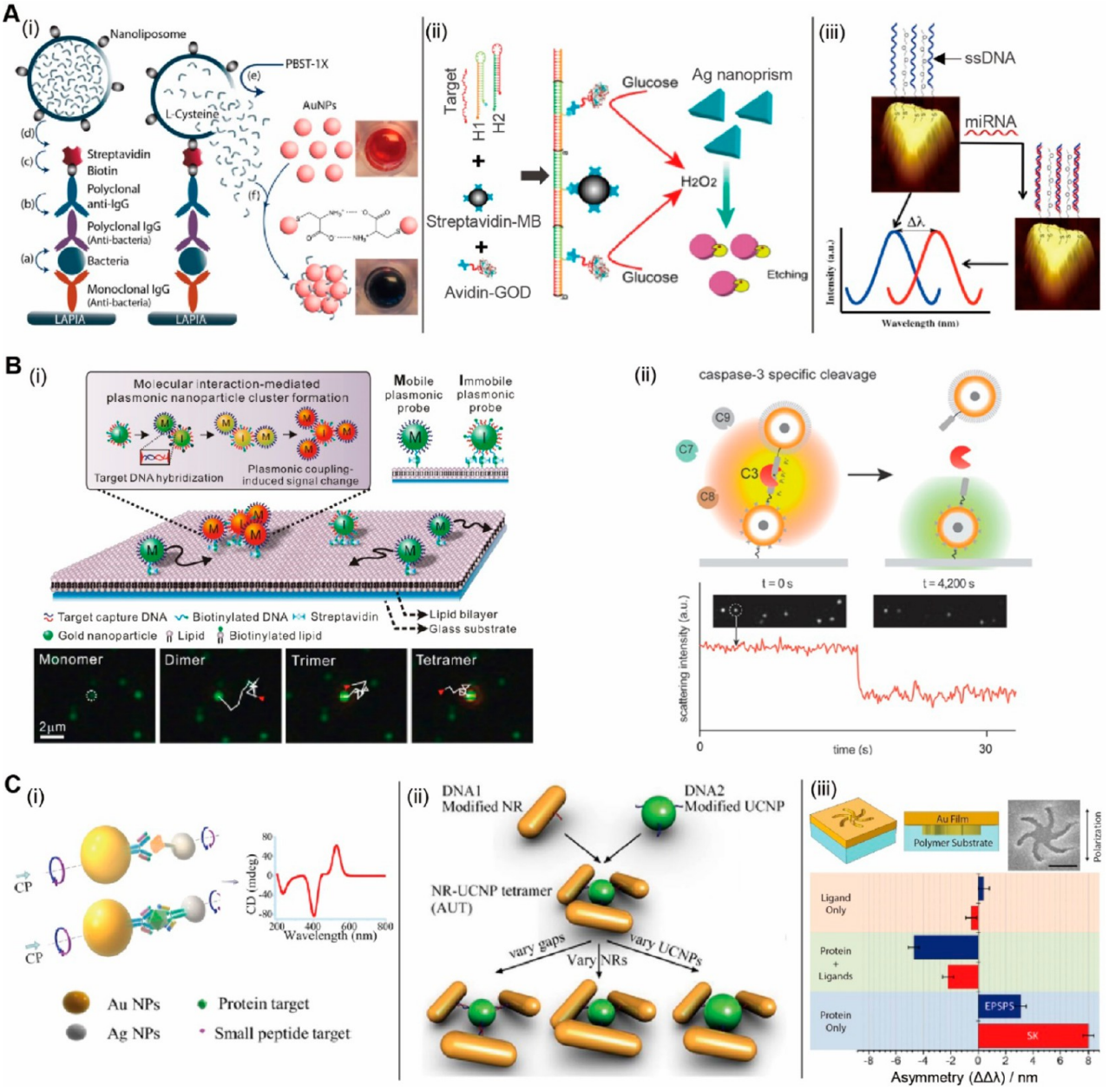

Figure 2. LSPR shift and Rayleigh scattering-based PEN biosensors. (A) LSPR shift-based biosensors: (i) liposome-amplified plasmonic immunoassay; (ii) construction of hybridization chain reaction-based specific DNA detection platform (the sensing mechanism is based on the etching process of triangular silver nanoprisms); (iii) ssDNA(target capture sequence)-functionalized Au nanoprisms attached to glass substrate for detecting miRNA target. (B) Dark-field light-scattering-based biosensing platforms: (i) dark-field scattering based single-particle-level imaging and detection of ssDNA target-mediated dynamic interactions among AuNPs on supported lipid bilayer; (ii) dark-field scattering-based monitoring of apoptotic drug-induced caspase-3 activity in leukemiacaspase-3 by selective cleavage of peptide-linking $Zn_{0.4}Fe_{2.6}O_4$@SiO_2@Au core−shell plasmonic NPs. (C) Chiroplasmonic sensors: (i) plasmonic chiral assembly of an Au−Ag heterodimer via target protein detection and resulting CD response; (ii) propeller-like nanorod-upconversion NP assemblies for DNA chiroplasmonic sensing; (iii) graphical depiction of left-handed chiral plasmonic Shuriken nanostructure and its SEM image (scale bar =250 nm). $\Delta\Delta\lambda$ values shown in this figure were obtained from the optical rotatory dispersion (ORD) spectra of shikimate kinase and 5-enolpyruvylshikimate 3-phosphate synthase with and without ligands, where $\Delta\Delta\lambda = \Delta\lambda_R - \Delta\lambda_L$ ($\Delta\lambda_R$ and $\Delta\lambda_L$ are resonance wavelength shifts measured on right-handed and left-handed Shuriken nanosubstrates, respectively). Images were reproduced with permission from (A) ref 97, Copyright 2015 American Chemical Society (ACS); ref 98, Copyright 2014 ACS; ref 100, Copyright 2014 ACS; (B) ref 101, Copyright 2014 ACS; ref 102, Copyright 2014 ACS; (C) ref 114, Copyright 2013 ACS; ref 116, Copyright 2016 Wiley; ref 120, Copyright 2015 ACS.

3. PLASMONICALLY ENGINEERED NANOPROBES FOR BIOSENSING

Multifunctional probes for ultrasensitive detection of multiple disease biomarkers have always been in demand. Among the various biosensing methods, nanotechnology-based optical biosensors, especially with plasmonic nanostructures, have drawn substantial interest.[92,93] In addition to the common advantages of nanotechnology-based sensors, such as large surface area, versatile surface chemistry for bioconjugation, and biocompatibility, PENs have built-in signal transduction features because of their tunable LSPR-induced field enhancement, absorption, and scattering properties, and targets can be detected

DOI: 10.1021/jacs.6b09451
J. Am. Chem. Soc. 2016, 138, 14509−14525

with high sensitivity and selectivity, often in a multiplexed manner. Importantly, signal transduction for biosensing applications can be well controlled by tuning the size, shape, and assembly of the PENs. In this section, we describe recent advancements in biosensing methods involving PENs based on their LSPR, light-scattering, chiroplasmonic, SERS, and fluorescence-signal tunability.

3.1. PENs for LSPR-Based Biomolecular Sensing. Light can be coupled into standing or propagating surface plasmon modes through a grating, a defect or other surface features in the metal surface. LSPR-active structures can be used for sensing changes in the bulk refractive index of their environment by measuring the shifts in the LSPR peak wavelength.[94] LSPR-based biosensing nanoprobes have been developed by using target molecule-mediated aggregation, changes in nanoprobe morphology, and molecular interaction-mediated electronic perturbation shift in the LSPR absorption wavelength (Figure 2). Such LSPR-based nanoprobes exhibit advantages such as ease of operation with no need for labeling the target, fast assay time, and straightforward readout of detection signals. However, such LSPR-based biosensors are associated with non-specific binding of biomolecules, non-specific aggregation of NPs, narrow dynamic range of measurement concentrations, and non-recyclability of the nanoprobes. Moreover, the plasmonic properties of the resulting aggregated structures in these cases are often unpredictable and uncontrollable and offer a very narrow scope of pre-conceived designs and a limited dynamic range in target concentration.

Large aggregation of plasmonic NPs allows for colorimetric biosensing without a need for instrumentation for signal readout. Jiang et al. utilized alkaline phosphatase-triggered click-chemistry between azide/alkyne-functionalized AuNPs for colorimetric plasmonic immunoassay.[95] Such approaches do not require additional enzymes and the expensive instrumentation used in conventional immunoassays.[96] Recently, Abbas et al. achieved attomolar-level naked eye colorimetric detection of pathogens using a liposome-amplified plasmonic assay (Figure 2A-i).[97] In this case, the amplified response was initiated by buffer-triggered rupture of cysteine-loaded nanoliposomes and subsequent aggregation of AuNPs. High detection sensitivity can also be achieved by target-mediated shape modification of plasmonic NPs and the resulting quantitative LSPR shift.[98,99] A combination of enzyme-linked hybridization chain reaction amplification, H_2O_2-mediated etching of silver nanoprism, and subsequent LSPR shift was used to detect DNA at ~6 fM concentration and showed a high specificity (Figure 2A-ii).[98] Recyclability of diagnostic platforms is crucial for commercial applications, particularly when noble metals are integral parts of the sensor design. Sardar et al. developed a regenerative solid-state LSPR-based biosensing platform consisting of gold nanoprisms for microRNA (miRNA) detection at subfemtomolar concentration in the human plasma of cancer patients (Figure 2A-iii).[100] The simplicity of LSPR-based detection methods makes them attractive for commercial adaptation, but additional studies are still needed to design new PENs and advance existing LSPR-based diagnostic approaches for a wide and practical use of LSPR probes, especially for the above-mentioned issues.

3.2. PENs for Rayleigh Scattering-Based Biosensing. PENs can exhibit intense and controllable Rayleigh light-scattering properties, and scattering cross sections can be tuned by the shape and size of particles and the extent of plasmonic coupling. Two or more plasmonic NPs can be coupled together using biomolecules such as DNA or peptides, where the length of connecting molecules is the main factor in determining the distance between NPs. When two plasmonic NPs are brought into close proximity, the surface plasmon resonances of the individual NPs will couple, generating a light-scattering spectrum that depends on their interparticle distance.[43] Light confinement in nanometer-scale volume by PENs allows for high spatial resolution up to the single-molecule level because of the large-scattering cross section of metal NPs and resulting high intensity of the scattered spectrum. The light-scattering spectrum is typically time-invariant and can be continuously acquired in real time for long imaging periods. These signals can be detected with dark-field microscopy, where non-scattered light is removed to build an image only with scattered wave components against dark background. In contrast, conventional fluorescence-based single-molecule methods are prone to photobleaching, blinking, and low signal-to-noise ratios.

Recently, a photostable NP-modified supported lipid bilayer platform was developed for dynamic and quantitative dark-field microscopic imaging of plasmonic NP interactions mediated by ssDNA on a supported lipid bilayer (Figure 2B-i).[101] In this platform, individual particle-by-particle clustering processes were simultaneously monitored in real time and quantified by analyzing individual particle diffusion trajectories and single-particle-level plasmonic coupling. This highly reliable real-time analysis method on interactions between NPs on a 2D lipid platform allows not only for detecting fM-level DNA but also for differentiating single-base mismatch at a fM range. Such PEN-based analytical platforms may have versatile applications for detecting interactions including DNA, RNA, proteins, and chemical ligands and *in situ* monitoring of heterogeneous membrane reactions and receptor clustering. In another report, a pair of $Zn_{0.4}Fe_{2.6}O_4$@SiO_2@Au core−shell plasmonic NPs connected by a caspase-3 cleavage peptide sequence was used to monitor anti-cancer drug-induced caspase-3 activity during apoptosis (Figure 2B-ii).[102] The use of dielectric core ($Zn_{0.4}Fe_{2.6}O_4$@SiO_2)−shell (Au) structure provided more intense light-scattering compared to solid AuNPs, and the magnetic core helped in purification during plasmonic ruler assembly. Caspase-3 activity was monitored by the decrease in light-scattering intensity upon increase in interparticle distance and diminishing plasmonic coupling.

The expression levels of cell surface receptors play crucial roles in cell signaling under normal or disease conditions and can act as diagnostic hallmarks for a number of diseases. One of the most interesting applications of PENs is the detection and quantification of cell membrane receptors on sub-diffraction limit length scales.[103−105] Reinhard et al. successfully quantified the transmembrane proteins $ErbB_1$ and $ErbB_2$ in a variety of cancer cell lines using 40 nm AuNP immunolabels exhibiting interparticle distance-dependent differential plasmonic coupling upon increasing receptor density.[106] Upon increasing receptor density, AuNPs were positioned very close to each other within a strong plasmonic coupling interparticle distance range (<5 nm), causing detectable wavelength red-shifts and enhancements in the intensity of scattered light. The information regarding the expression of these transmembrane proteins is crucial for monitoring and diagnosing various malignancies. In an another report by Coronado et al., 90 nm AuNP immunolabels were used to determine the distribution and quantification of density of metabotropic glutamate receptor 1a on neuron cells at the sub-cellular scale.[107] In a recent report by Irudayaraj et al., plasmonic nanoprobes (50 nm Au and Ag NPs) were used for single-cell quantitative epigenetic profiling.[108] Utilizing hyperspectral dark-

DOI: 10.1021/jacs.6b09451
J. Am. Chem. Soc. 2016, 138, 14509−14525

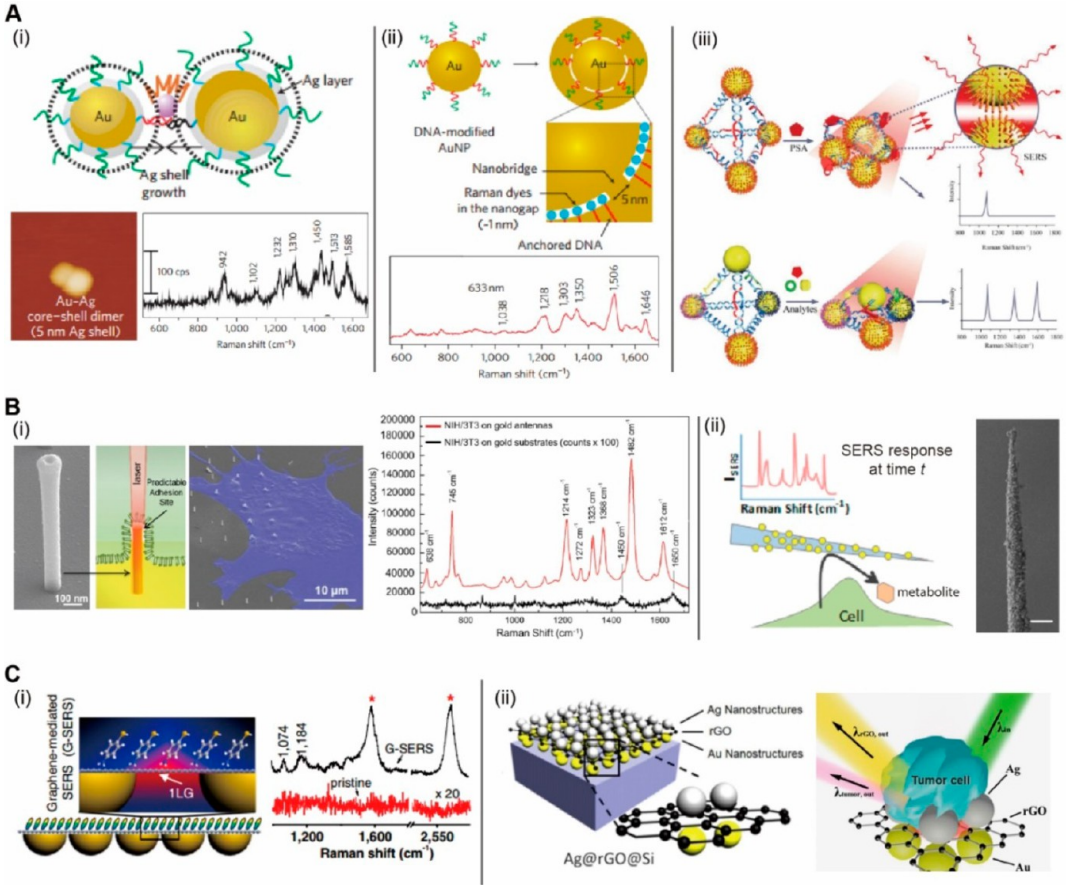

Figure 3. PENs for SERS-based biosensors. (A) Plasmonic nanogap-enhanced SERS biosensing probes: (i) Silver shell-based nanogap-engineering of a dimeric Au−Ag core−shell nano-dumbell for highly reliable single-DNA sensing; (ii) Au-nanobridged nanogap particles (Au-NNPs) with ∼1 nm interior nanogap for highly uniform, reproducible SERS signal generation; (iii) DNA frame-based formation of a Ag pyramid and its use for SERS biosensing. (B) Out-of-plane plasmonic antennas as a nano-endoscope for SERS-based live cell molecular analysis on the cellular membrane (i) and SERS-based nano-pipet for monitoring cell secretion events from living cells in extracellular environment (ii). (C) Graphene-engineered SERS substrates: (i) G-SERS substrate built from graphene and gold nano-hemispheres for molecular detection; (ii) Design of G-SERS substrate built from rGO sheets sandwiched between AuNPs and AgNPs for live cell analysis. Images were reproduced with permission from (A) ref 41, Copyright 2010 Nature Publishing Group (NPG); ref 125, Copyright 2011 NPG; ref 129, 2015, Copyright Wiley; (B) ref 130, 2015 Copyright Wiley; ref 133, 2016 Copyright ACS; (C) ref 139, Copyright 2012 National Academy of Science (USA); ref 135, 2016 Copyright NPG.

field imaging, the detection of low-level cytosine modifications under different conditions, such as in different cell lines, at different cell phases, and even on a single chromosome, was achieved. Unlike fluorescence-based imaging methods, PEN-based methodology effectively circumvents limitations such as low resolutions, signal instability, and complex instrumentation. The research groups of Bissell and Alivisatos reported a reversible plasmon ruler, comprised of coupled AuNPs (30 nm) linked by a single aptamer (MMP-3 aptamer), capable of binding individual cell-secreted molecules (MMP-3) with high specificity.[109] Quantification of secreted single molecules from cells, such as growth factors, proteases, and morphogens, within 3D cellular microenvironments can provide insight into how tissues form and become patterned during development and may suggest therapeutic strategies for repairing diseased tissues. PEN light-scattering tags offer such a simple, convenient, and reliable method for observing single molecules and corresponding biochemical events using relatively cheap benchtop dark-field microscopy setups, which are typically quite challenging to achieve. However, more advanced PEN probes should be designed and synthesized with better sensitivity, improved data reproducibility, and multiple light-scattering color profiles, and well-controllable, reliable bioconjugation chemistry for varying nanostructures is needed to exploit the multiplexing capability of light-scattering PENs.

3.3. PENs as Chiroplasmonic Sensors. A large variety of biomolecules such as sugars, nucleic acids, and proteins have inherent characteristic chirality. Understanding corresponding chiral information is crucial for the mechanistic evaluation of biochemical reactions. Circular dichroism (CD) spectroscopy can be used to determine chiral information about bioanalytes including tertiary and quaternary structures; however, its application in biosensing is limited by low sensitivity and requirement of UV radiation to excite chiral biomolecules. Plasmonic metal NPs such as AgNPs can enhance CD signals arising from a comparable enhancement of the overall electronic absorption of specific probe molecules on AgNPs, where the metal surface plasmons are in resonance with the molecular electronic transition.[110] Chiroplasmonic coupling results in a new CD band in the visible light wavelength range via two possible mechanisms: either plasmonic electrons induce a change in the electromagnetic field inside chiral molecule or the chiral molecule induces a chiral current in the plasmon.[111−113] The origin of this new CD band in the visible range enables CD-based biodetection using visible light. The assemblies of achiral plasmonic NPs in a stereo-controlled fashion generate chiral

DOI: 10.1021/jacs.6b09451
J. Am. Chem. Soc. 2016, 138, 14509−14525

geometries (such as tetrahedral and helical arrangements), and the corresponding plasmonic CD response can be used as a diagnostic signal for biosensing applications.

Homo- and heterodimers of spherical NPs are typically considered to be achiral because of their basic symmetry configuration; however, Kotov et al. reported chiral Au−Ag heterodimers assembled from protein target capture between complementary biomolecule-functionalized Au and Ag NPs (Figure 2C-i).[114] The chiroplasmonic properties of such dimeric assemblies are attributed to the prolate shape of individual NPs and resulting scissor-like geometry with the protein target bridge. The strong polarization rotation in these nano-assemblies was utilized to detect an environmental toxin, microcystin-LR, and a cancer biomarker (e.g., prostate-specific antigen). Deposition of gold and silver shells around the scissor-like conformationally chiral DNA-bridged PEN dimers enabled spectral modulation of their chiroplasmonic bands in the 400−600 nm region and resulted in significantly enhanced optical activity; such PENs enabled polymerase chain reaction-based DNA detection at the zeptomolar level.[115] Chiral propeller-like PEN, assembled from AuNR and upconversion NP linked with hairpin DNA (hpDNA) which has intense chiroptical activity, has been used for plasmonic CD signal- and luminescence signal-based detection of DNA targets (Figure 2C-ii).[116] In the presence of DNA targets, hpDNA strands of the tetramers were extended because of their specific biorecognition, resulting in a wider plasmonic gap, which reduced both luminescence and CD signal intensities. Chiroplasmonic nanopyramids self-assembled from gold and upconversion nanoparticles (Au-UCNPs) have been used for ultrasensitive quantification of miRNA in living cells.[117] The Au-UCNP pyramids have dual signaling mechanisms, strong plasmonic CD at 521 nm, and significant luminescence at 500−600 nm. Upon exposure to miRNA, the CD signal was decreased, and luminescence intensity was increased. Thus, the CD signal was much more sensitive to the concentration of miRNA than the luminescent signal because of the strong CD intensity arising from the spin angular momentum of the photon interaction with chiral nanostructures and plasmonic enhancement of the intrinsic chirality of DNA molecules in the pyramid geometry. Specifically designed nano-metamaterials possess a variety of inherent chiralities (such as helical chirality, axial chirality, and supramolecular chirality) because of the concentration of superchiral electromagnetic fields in their vicinity;[118] such PENs can sensitively detect a variety of chiral biomolecules.[119,120] Recently, Kadodwala et al. demonstrated the potential of plasmonic superchiral polarimetry using a templated chiral plasmonic nanostructure (shuriken-like shape). This can rapidly characterize ligand-induced changes in protein tertiary and quaternary structures with high sensitivity, which is undetectable using conventional CD spectroscopy (Figure 2C-iii).[120]

3.4. PENs for SERS-Based Biodetection and Bioprobing. Recently developed SERS-based plasmonic biosensors show great potential in practical and wide use for biodetection with well-designed and synthetically controlled PENs. The origin of SERS is attributed to the complex effect of electromagnetic and chemical enhancement mechanisms.[121,122] SERS offers tremendous potential for highly sensitive, multiplexed molecular detection with chemical structural molecular fingerprinting. Using well-designed Raman nanoprobes, it is possible to detect analytes with a limit of detection up to the single-molecule level.[123,124] The performance of conventional SERS techniques greatly depends on the distribution and control of hot-spots on SERS substrates such as rough Au, Ag surfaces, or in random assemblies of NPs with interparticle plasmonic gaps where hot spots are located. The geometries and locations of hot-spots in such conventional substrates are not well-controlled, and therefore the signals are often not strong or reliable. Discrete PENs with localized, ultrastrong electromagnetic fields have emerged as widely used SERS-substrates for single-molecule and ultrasensitive SERS detection because the Raman signals are amplified by many orders of magnitude. It was shown that DNA-linked dimeric plasmonic nanogap-enhanced Raman-scattering nanoprobes (nano-dumbbells) with a highly tunable narrow gap size (∼1 nm) and ultrastrong EM field have a single-molecule level Raman detection capability and high signal reproducibility (Figure 3A-i).[41,81,125−128] Well-controlled chemistry in modifying thiolated oligonucleotides and growing AgNS on Au core with a plasmonic nanogap is crucial for achieving reliable and highly sensitive SERS signals; the plasmonic gap should be sufficiently small to maximize the EM field and SERS signals but not cause quantum tunneling, which abruptly ceases the EM enhancement when the gap size becomes too small (e.g., ∼0.3 nm or smaller). The number and precise positioning of Raman reporter molecules in a "hot-spot" region are also crucial for obtaining reproducible, quantifiable Raman signals. Careful control of these factors for designing PENs is of paramount importance for applications in SERS-based biosensing and bioimaging. Gold nanobridged nanogap particles (Au-NNPs) with ∼1 nm interior gap exhibited strong SERS signals (EF value of $>1.0 \times 10^8$) with high structural uniformity and signal reproducibility.[123] In the Au-NNP probe design, ssDNA-tethered Raman reporters are precisely located in the uniformly formed 1 nm plasmonic gap inside particles (Figure 3A-ii). In a report by Xu et al., nanopyramids built from a DNA frame and AgNPs were used to detect attomolar quantities of a variety of disease biomarkers (Figure 3A-iii).[129] The DNA frame was embedded with a biomarker-specific aptamer; upon reacting with the biomarker, the AgNP nanopyramid is collapsed and AgNPs come very close, which causes strong plasmonic coupling resulting in SERS-based sensitive detection of subjected biomarkers.

Recently, interest has increased in probing real-time extracellular and intracellular biomolecular information using SERS-based PENs in living cells. A 3D SERS substrate with vertical plasmonic nano-antennas protruding from the substrate plane has been used for the chemical analysis of living fibroblasts in NIH/3T3 cells (Figure 3B-i).[130] The tight adhesion between cells and plasmonic antennas enabled sensitive SERS analysis of cell membrane elements at well-defined and predictable points. The potential of nanosized plasmonic endoscopes such as silver nanowires and AuNP-decorated carbon nanotubes has been demonstrated for SERS-based molecular analysis inside living cells.[131,132] However, the control and modification of hot-spot geometries for enhanced sensitivities and modification with targeting moieties for selective biomolecular detection in different parts of the live cell require further advancements. A nanopipette decorated with AuNPs has been used for SERS-based monitoring of metabolite (such as pyruvate, lactate, ATP, and urea) secretion in Madin-Darby canine kidney epithelial cells (Figure 3B-ii).[133] In *in vivo* models, such real-time monitoring can be useful for evaluating organ health in normal and disease conditions. Graphene is important in material science because of its atomic thinness and unique and useful optical, electronic, and mechanical properties. A combination of graphene and plasmonic nanostructures has been utilized in a variety of

DOI: 10.1021/jacs.6b09451
J. Am. Chem. Soc. 2016, 138, 14509−14525

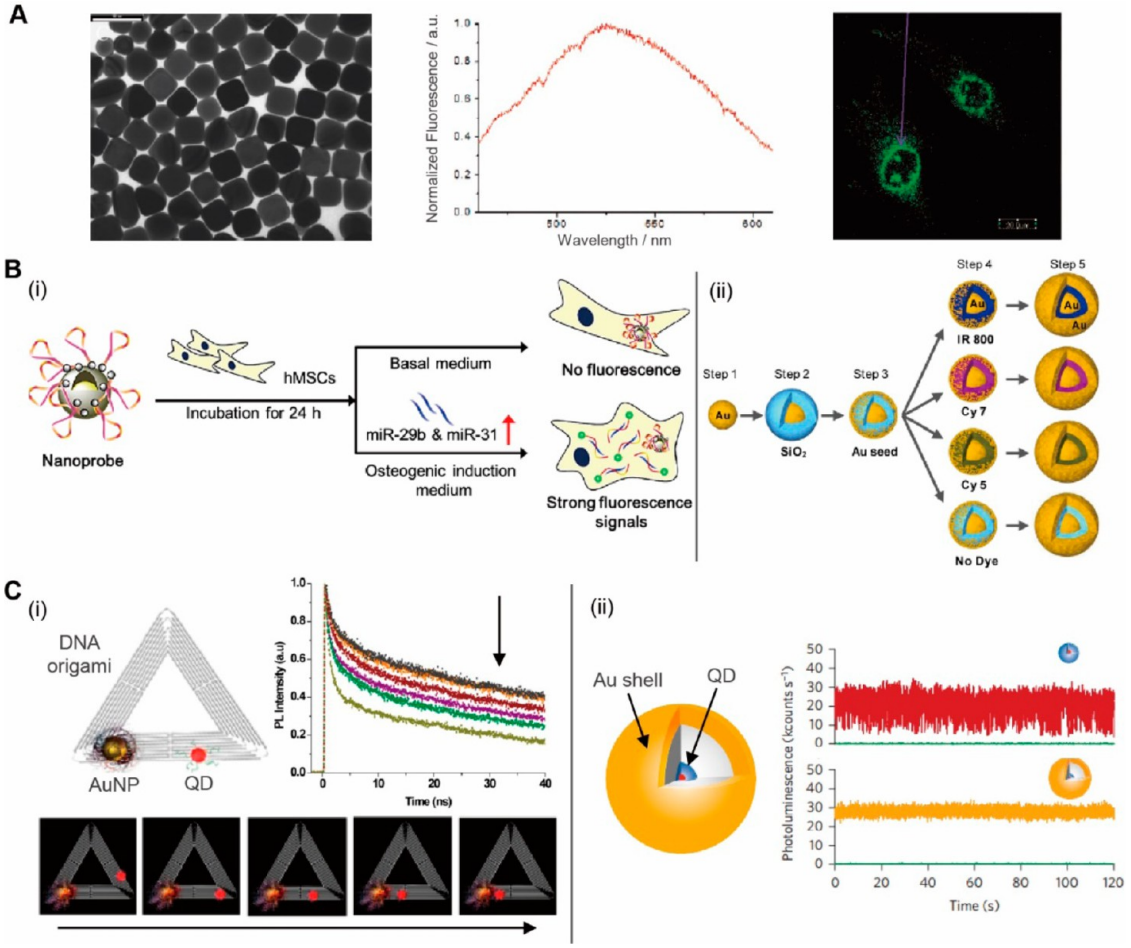

Figure 4. Photoluminescent and fluorescence quenching/enhancing PENs. (A) Au nanocubes for PL-based bioimaging: TEM image of Au nanocubes (left), fluorescence spectrum of cells (middle), and fluorescence image of cells (right). (B) Fluorescence quenching (i) and enhancing (ii) PENs: (i) intracellular detection of miRNAs in human mesenchymal stem cells (hMSCs) using polydopamine-coated AuNPs with fluorophore-modified hairpin-DNA; (ii) nano-matryoshka with embedded fluorophores inside the silica interlayer and fluorescence enhancement. (C) Quantum dot(QD)-PEN hybrids: (i) DNA origami template-based quenching of QD fluorescence by controlling the distance between QD and AuNP; (ii) plasmonic nanoshell resonator for obtaining non-blinking fluorescence from QDs. Images were reproduced with permissions from (A) ref 149, Copyright 2010 ACS; (B) ref 152, Copyright 2015 ACS; ref 158, Copyright 2014 ACS; (C) ref 162, Copyright 2014 ACS; ref 163, Copyright 2015 NPG.

SERS-based applications (Figure 3C). Although graphene has been found to possess intrinsic moderate Raman signal-enhancing properties through a charge-transfer mechanism with reporter molecules, using graphene alone as an SERS substrate is limited because of its low sensitivity.[134] Recently, the use of graphene as an atomically thin separator between plasmonic NPs was shown to form a very narrow plasmonic gap for generating strong, controllable electromagnetic field and SERS signals inside the gap.[135−138] Moreover, the flat 2D surface of graphene can be used to locate analyte molecules homogeneously present throughout the large SERS substrate, which is crucial for the reproducibility of SERS signal measurements.[139] The D and G bands from graphene can be used as diagnostic bands for locating hot-spot regions in large plasmonic substrates, and also chemical enhancements act synergistically with electromagnetic enhancement.[140,141]

To obtain high spatial resolution, scanning probe microscopy such as atomic force microscopy was combined with SERS to develop the tip-enhanced Raman spectroscopy (TERS).[142] In TERS, the scanning probe microscopy tip is typically modified with nanosized (~20 nm) plasmonic metals (Au or Ag) to generate a hot-spot junction between the tip and substrate, resulting in sensitive molecular profiling of the analyte on the substrate with reasonably good spatial resolution (~10 nm). Because only one hot-spot can be typically generated at a time for Raman spectroscopic measurements, the sensitivity of the method is compromised. However, the TERS plasmonic tip can be engineered with a suitable arrangement of NPs to enhance the sensitivity.[143] TERS has been successfully used for the molecular profiling of cell surfaces, viruses, and isolated biomolecules. Recently, a TERS setup with an atomic force microscopy tip plasmonically engineered with closely assembled 14 nm AuNPs was applied for chemical imaging of *Bacillus subtilis* spores, which revealed a dense arrangement of both proteins and carbohydrates on specific spore surface regions.[144] Such detailed molecular information is useful for bacterial surface-display systems and drug delivery applications. Molecular probing of hemozoin crystals in the digestive vacuole of a sectioned malaria parasite-infected cell by TERS revealed spectral features consistent with a five-coordinate high-spin ferric heme complex.[145] Detailed molecular profiling of the hemozoin crystal will be helpful for drug screening to identify drugs that can bind to the hemozoin surface within the digestive vacuole of the malaria trophozoite. The spatial molecular probing capability of

DOI: 10.1021/jacs.6b09451
J. Am. Chem. Soc. 2016, 138, 14509−14525

TERS is useful for obtaining spectroscopic information from the selected regions of the sample and cutting out the background from bulk samples, as demonstrated in the detection of nano-oxidation sites on the surface of hemoglobin crystals.[146]

Overall, plasmonic nanostructure-based SERS has a wide range of applications in biomolecular detection and real-time monitoring of biochemical reactions, with great potential in the fields of genomics and proteomics. Emerging sophisticated PENs with high signal enhancement factors and breakthroughs in synthetic methods for obtaining targeted PENs in a high yield may open new directions for ultrasensitive biodiagnostic platforms such as for early-stage cancer diagnosis and multiplexed profiling of multiple biomarkers; however, the fabrication of such SERS substrates with high reproducibility requires further analysis and validation, especially for clinical applications of these platforms.

3.5. PENs as Photoluminescent Probes and Fluorescence Quenching or Enhancing Substrates. Metal NPs intrinsically exhibit weak photoluminescence (PL) upon photon excitation due to the low probability of radiative recombination of relaxing electron−hole pairs. However, suitable tuning of SPR and enhancement in local field can result in an enhancement in PL quantum yield. Many interesting features of plasmonic metal NPs, such as large light absorption cross section and non-photobleaching and non-photoblinking behaviors, make them attractive alternatives to conventional organic fluorophores for biomedical applications. Moreover, this PL-based visualization of NPs is a straightforward, reliable, and versatile approach for studying and characterizing nanoprobes in biosensing, bioimaging, and therapeutic applications. AuNRs have been extensively studied for one-photon and two-photon luminescence, where excitation laser wavelength is coupled with longitudinal LSPR energy.[147] It has been observed that nanostructures with sharp edges, such as gold nano-bipyramids and gold nanocubes, can show enhanced quantum yield of PL due to the "lightning-rod effect".[148,149] Particularly, gold nanocubes with sharp edges and LSPR band close to the interband transition energy show a high PL quantum yield, 200 times higher than for AuNRs. Chen et al. utilized gold nanocubes for PL-based bioimaging of QGY and 293T cells (Figure 4A).[149]

Plasmonic metal NPs are known to quench the fluorescence of organic molecules and quantum dots depending on the size and proximity of NPs, known as nanometal surface energy transfer (NSET).[150,151] Mechanistically, NSET is similar to Förster resonance energy transfer (FRET), where two closely positioned oscillating dipoles interact with one another and energy is transferred from the excited state of a donor molecule to the ground state of the acceptor molecule via a non-radiative pathway. FRET is useful for measuring intermolecular distances that are 1−10 nm. However, NSET can measure intermolecular distances up to 50 nm, depending on the size and shape of metal NPs. This longer-range effect in NSET occurs because of the large size and high polarizability of plasmonic NPs relative to the small fluorescent molecules. Recently, Bian et al. utilized the recovery of quenched fluorescence of a hpDNA-tethered fluorophore on the surface of polydopamine-coated AuNPs as a biosensing switch for detecting miRNA in living human mesenchymal stem cells (hMSCs) (Figure 4B-i).[152] These fluorophore-modified PENs efficiently entered the cell and provided information on miRNA in real time only in the hMSCs undergoing osteogenic differentiation, and living primary osteoblasts specifically. Unlike conventional organic dye-based probes, the signals from Au@PDA−hpDNA PENs could be monitored for 5 days without any additional treatment of cells with the probes. Such robust PENs can be used for monitoring long-term dynamics of a variety of stem cells during differentiation processes. Liu and co-workers have developed fluorophore−AuNP hybrid probes for Hg^{2+} detection in living cells.[153] In the probe design, fluorescent dyes were closely tethered to AuNP surface by isothiocyanate linkers to quench fluorescence signal. Upon exposure to Hg^{2+} ions, the dye molecules were distantly located from the AuNP surface resulting in the enhancement in fluorescence signal.

Fluorescence-based detection and imaging are typically limited by quantum yield, autofluorescence of samples, and/or the photostability of fluorophores. Plasmonic metal surfaces can increase or decrease the radiative decay rates of fluorophores depending on the position of the fluorophore with respect to the metal surface.[82] In recent years, metal-enhanced fluorescence (MEF) has gained significant attention for its optical properties and biomedical applications. For practical applications of MEF probes, it is critical to engineer the geometry and size of metal NPs and the distance between the fluorophore and metal NP surface for generating stronger, more stable fluorescence signals. Halas et al. reported PENs such as AuNS and AuNR in which silica or human serum albumin serves as a spacer layer between NP and fluorophore.[154−156] In a report by Orrit et al., the fluorescence of a weak emitter, crystal violet, was enhanced >1000-fold by a single AuNR under the resonant condition.[157] Sophisticated PENs such as nano-matryoshkas, consisting of an Au core, interstitial nanoscale SiO_2 layer, and Au shell layer, were reported to cause either a strong enhancement or quenching of the fluorescence emission from the fluorophores dispersed within the internal dielectric layer (Figure 4B-ii).[158] The strong MEF effect in nano-matryoshkas has been proposed to originate from near-field enhancement induced by Fano resonance. Xia et al. utilized the micropatterned Au nanocages for NIR light-induced MEF of organic dyes with 2−7-fold signal enhancement.[159] The potential of MEF probes in biosensing has been demonstrated by Dai et al. in the detection of islet cell-targeting autoantibodies (an early stage biomarker for diagnosing type-I diabetes) on fluorescence-enhancing, nanostructured plasmonic gold chips. Integration of plasmonic Au chip onto a conventional antibody−antigen sandwich assay allowed ∼100-fold increase in detection sensitivity of target biomarkers.[160] The methods involving plasmonic chips were also extended to the MEF-based detection of multiple cellular proteins in different types of single cells through a microarray of the cells, which is useful for potentially hundreds to thousands of different types of cells assayed on a single chip.[161]

Liu et al. demonstrated the dependence of QD fluorescence emission on the proximity of 30 nm AuNPs with controlled interparticle distances of 15−70 nm.[162] This was achieved by co-assembling DNA-conjugated QDs and AuNPs in a 1:1 ratio at precise positions on a triangular-shaped DNA origami platform (Figure 4C-i). Such long-range fluorescence quenching phenomena could be useful for developing advanced spectroscopic rulers that overcome the limitations of FRET. Although toxicity issues exist for biomedical applications of QDs, QDs have been known for stronger signals, sharper emission peaks, and more stable signals than conventional organic dyes. However, the fluorescence signals of QDs occasionally fluctuate due to their chemical reactivity to the environment and non-radiative Auger recombination upon during relaxation. Dubertret et al. have addressed the shortcomings of QDs by coating the QD with silica followed by the formation of Au shell resulting in a QD/silica/Au

DOI: 10.1021/jacs.6b09451
J. Am. Chem. Soc. 2016, 138, 14509−14525

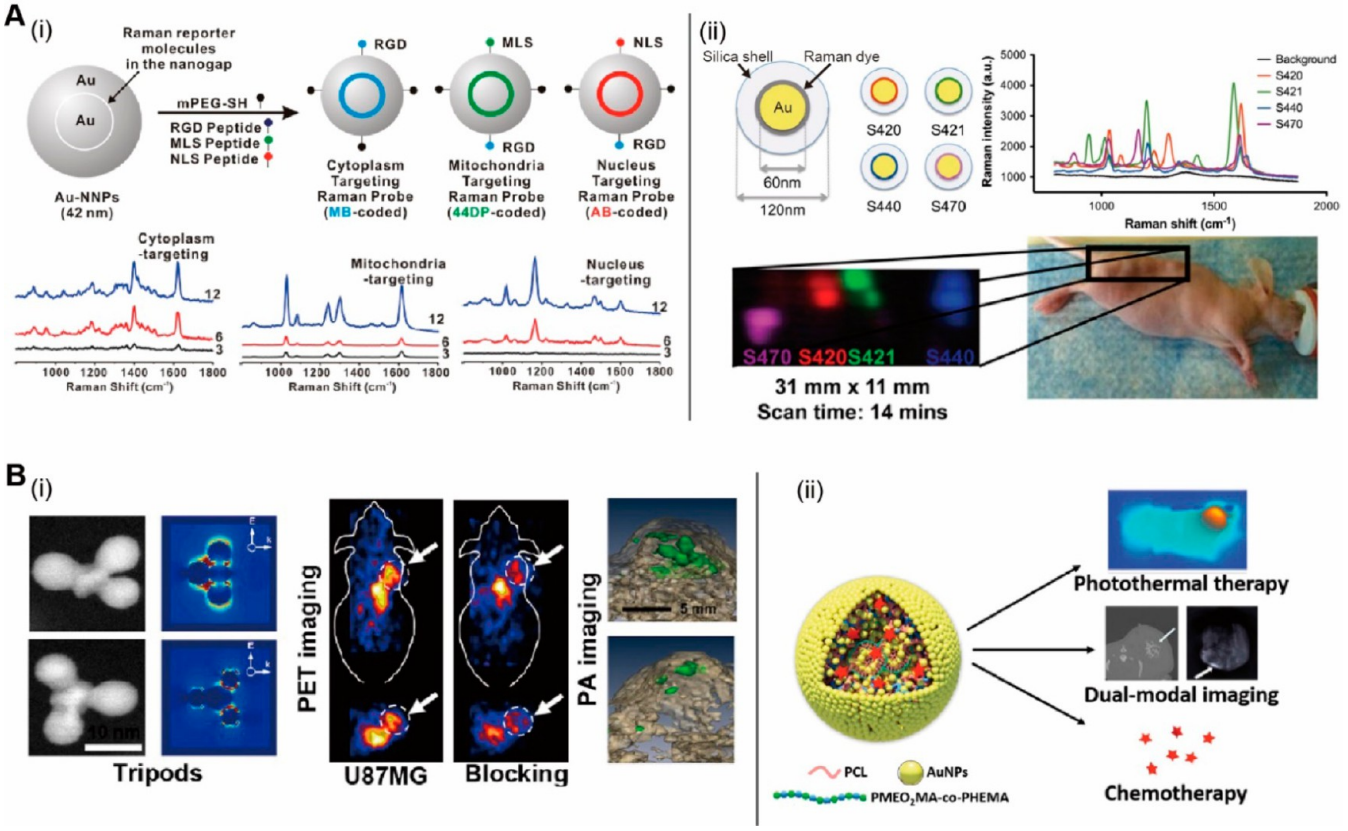

Figure 5. PENs for bioimaging (A) SERS tags for bioimaging: (i) SERS Au-NNPs functionalized with targeting ligands for different organelles and encoded with different Raman reporters and targeted cell imaging with Au-NNPs; (ii) SERS nanotags for *in vivo* bioimaging. Raman dye encoded-silica coated AuNPs with a 60 nm diameter gold core and Raman mapping of the mouse with four different types of SERS nanotags (S420, S421, S440, and S470). (B) Au tripods with a Pt nanocube core for photoacoustic tumor imaging (i); Au nanomicelle for multimodal bioimaging (X-ray computed tomography and photoacoustic tomography) of tumor in mouse and photothermal and chemotherapy (ii). Images were reproduced with permissions from (A) ref 166, Copyright 2015 ACS; ref 167, Copyright 2013 National Academy of Science (USA); (B) ref 168, Copyright 2014 ACS; (C) ref 169, Copyright 2015 Wiley.

hybrid system (Figure 4C-ii).[163] The gold shell not only protects the QD from the outer environment but also enhances its resistance to high excitation energy, providing very stable fluorescence signals.

4. PLASMONICALLY ENGINEERED NANOPROBES FOR BIOIMAGING

It is important to monitor and map various processes at the cellular level such as cell proliferation, apoptosis, cell−cell communication, biochemical signal transduction, gene expression, and disease-specific receptor expression, among others. *In vivo* bioimaging of tumors is one of the most important topics in nanomedicine and biomedical engineering for early, accurate tumor diagnosis and imaging-guided surgery and therapy. Conventional methods for bioimaging such as X-ray, PET, single-photon emission CT, and magnetic resonance imaging (MRI) use high-energy radiation, radioactive waves, high magnetic fields, and toxic chemical contrast agents. Moreover, no single technique is sufficient for detecting a disease in early stages because of limited sensitivity and low resolution. PENs can offer a variety of imaging modules including SERS, MEF, PA imaging, and X-ray CT. These methods have several advantages over conventional methods, such as non-invasiveness, use of safe excitation light source (typically NIR light), better contrast, long-time monitoring, and multiplexing capability. As discussed above, a concentrated electromagnetic field near PEN dramatically enhances the fluorescence and Raman signals.

A PEN with a high absorption coefficient of NIR light converts into heat-generating PA waves for PA imaging with high spatial resolution. The attenuation of X-rays by PEN makes them efficient X-ray CT contrast agents. Radioactive species-labeled PENs can be imaged using PET, which is used to quantify and study the biodistribution and clearance of the nanoprobes but shows low spatial resolution.[164] Engineering particle size and surface to increase the number of ligands and radioactive labels per probe and to minimize non-specific binding has been proven useful in targeting tumor sites in a more efficient manner while maximizing excretion of nanoprobes.[165] SERS-based bioimaging is very promising because of its molecular fingerprinting capability, high spatial resolution, and good signal stability over time; however, low tissue penetration of excitation light, long acquisition time, and small field of view are major limitations to its wider applications. Lim et al. used AuNPs with an ∼1 nm interior nanogap and Raman reporters located precisely in the nanogap (Au-NNPs) for high-resolution and high-speed (30 s) live-cell Raman imaging parallel at multiple organelle levels (Figure 5A-i).[166] They found that highly sensitive SERS-active nanoprobes could provide high-resolution Raman-based cell images to reveal detailed cell dynamics under a variety of physiological conditions inside the cell. Gambhir et al. developed a wide-area (>6 cm^2) Raman bioimaging platform for *in vivo*

DOI: 10.1021/jacs.6b09451
J. Am. Chem. Soc. 2016, 138, 14509−14525

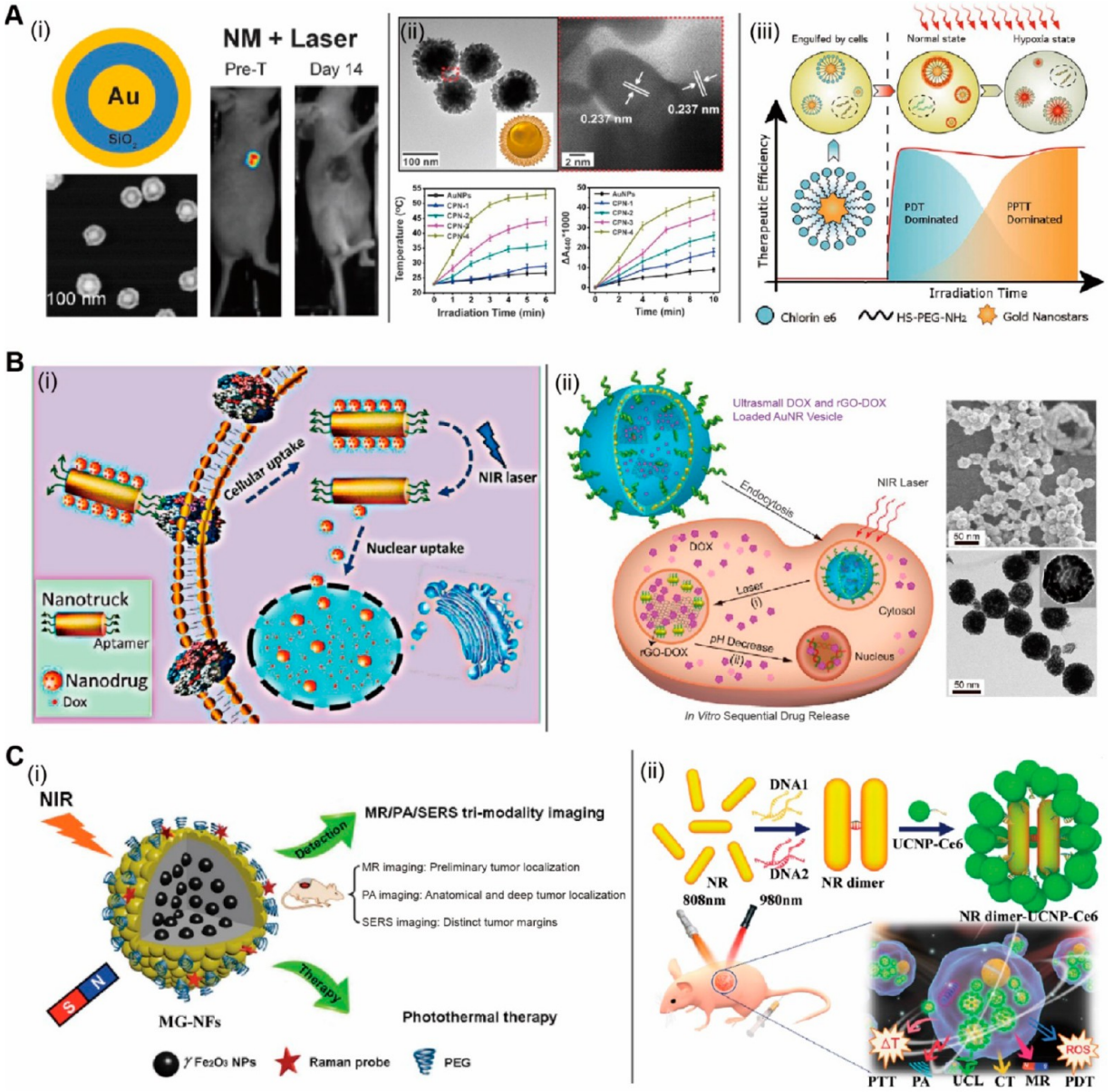

Figure 6. PENs for therapeutic and theranostic applications. (A) PENs for NIR-mediated phototherapy: (i) Au nano-matryoshkas for photothermal therapy; (ii) Au core−petal nanoprobes for dual photothermal and photodynamic therapy; (iii) Au nanostar−PEG−Ce6 conjugate used for dual photothermal−photodynamic therapy. (B) NIR laser-induced delivery of drugs: (i) Cell-targeted photocontrolled nuclear-uptake nanodrug delivery system (8.5 nm NP-AuNR assembly) for cancer therapy; (ii) DOX- and rGO-DOX-loaded AuNR vesicles for NIR light-mediated drug release inside cells. (C) Theranostic PENs: (i) SERS-MR-PA trimodal imaging and photothermal therapy with magnetic Au nanoflowers; (ii) upconversion-CT-PA-MR multimodal imaging and photothermal/photodynamic therapy using nanorod dimer and upconversion NP core−satellite assemblies. Images reproduced with permissions from (A) ref 182, Copyright 2014 ACS; ref 87, Copyright 2014 ACS; ref 178, Copyright 2013 Wiley; (B) ref 187, Copyright 2014 ACS; ref 188, Copyright 2015 ACS; (C) ref 194, Copyright 2016 Wiley; ref 90, Copyright 2016 Wiley.

applications using silica-coated AuNP Raman tags; this Raman imaging system can detect multiplexed SERS signals in both superficial and deep tissue locations (Figure 5A-ii).[167] Cheng and others reported gold nanotripods with a Pt nanocube core for PA-based bioimaging of tumors in mice (Figure 5B-i).[168] The gold tripod structure showed a large absorption cross section in the NIR region for PA imaging with high spatial resolution. Taking advantage of the versatile properties of PENs, various types of multimodal imaging nanoprobes with synergetic effects were developed. Zhang group reported gold nanomicelles for multimodal PAT/X-ray CT tumor bioimaging (Figure 5B-ii).[169] In the probe design, 6 nm AuNPs and biocompatible amphiphilic polymers were self-assembled into gold nanomicelles with high NIR absorption. After treatment, the gold nanomicelles were dissociated into single AuNPs with no cytotoxicity and enhanced clearance, which is crucial for wider *in vivo* applications. Because of their versatile surface chemistry, PENs can also be conjugated with other imaging agents to provide high levels of multimodality for bioimaging applications.

5. PLASMONICALLY ENGINEERED NANOPROBES FOR THERAPEUTIC AND THERANOSTIC APPLICATIONS

PENs are appealing for their diverse therapeutic applications such as non-invasive and benign cancer therapy. The photothermal properties of PENs have been widely studied for killing

DOI: 10.1021/jacs.6b09451
J. Am. Chem. Soc. 2016, 138, 14509−14525

cancer cells *in vitro* and *in vivo*. Under light illumination, the photon excites electrons in the PEN, and the excited electrons relax through radiative decay or non-radiative decay. The non-radiative decay produces heat by electron−phonon and phonon−phonon couplings. Efficient energy transfer from light into heat of PENs with high absorption cross section in the NIR region makes PENs a promising therapeutic agent. PTT involves hyperthermia, which is a moderate rise in body tissue temperature. Hyperthermia conditions induce subcellular events, including critical damage to proteins and cell membranes, leading to cell death. Tumor cells are more susceptible to temperature increase than normal cells because of their low oxygen and nutrient supply through immature blood vessels.

Anisotropic rod structures are excellent PTT agents, exhibiting strong longitudinal peaks in the NIR region that can be tuned by increasing the aspect ratio.[170] AuNSs[171,172] synthesized on silica core and gold nanocages[173,174] synthesized by galvanic replacement of a silver nanocube were extensively studied for PTT applications. The LSPR peaks of AuNSs and gold nanocages are tunable in terms of their size and ratio of outer shell radii to inner shell radii.[175,176] Upon increasing the particle size and decreasing plasmonic shell thickness to give a higher core-to-shell ratio, the LSPR peak shifted to longer wavelengths, ranging from visible to NIR. Gold nanostars[177−179] and other branched structures[180,181] exhibit high photothermal conversion efficiency because of the plasmonic coupling of multiple sharp edges with a high absorption-to-scattering ratio. The groups of Halas and Joshi reported 90 nm diameter Au nano-matryoshkas for PTT of cancer and found better *in vivo* therapeutic effects compared to the benchmark 150 nm diameter AuNSs (Figure 6A-i).[182] PENs can kill tumor cells via other mechanisms, such as PDT, by the generation of reactive oxygen species (ROS) under light illumination. PENs can function as PDT agents because light-induced excited electrons are transferred to O_2 to generate singlet oxygen, which promotes cell apoptosis or necrosis. We reported multifunctional gold core-petal nanoprobes that induce dual photodynamic and photothermal therapeutic effects without the need for organic photosensitizers (Figure 6A-ii).[87] PTT/PDT dual-modal treatment improved the efficiency of therapy with a low power of laser illumination and benign increase in tissue temperature, causing minimal damaging effects in healthy tissues. This type of PENs are suitable for PTT/PDT applications because of its high solubility, good photostability, tumor targeting ability, high absorption cross section, and efficient photothermal conversion. Gao et al. demonstrated that suitably controlled laser irradiation conditions for gold nanocages generated ROS, resulting in apoptotic cancer cell death, while more damaging hyperthermia effects were avoided.[86] PENs such as gold nanorings have also been demonstrated to enhance the generation of ROS from organic photosensitizer molecules activated upon release of the photosensitizers from and in the immediate vicinity of the AuNRs during NIR irradiation.[183] Hybrid systems of PENs and organic photosensitizer molecules have also been reported for cancer PTT−PDT platforms (Figure 6A-iii).[178] It should be noted that the size of therapeutic or diagnostic nanoprobes is a major concern for real biomedical applications because of their stability, poor biodistribution, and difficulty in renal excretion after use when particle size is large. Recently, Liu et al. reported highly stable, ultrasmall (<10 nm) Fe_3O_4@$Cu_{2-x}S$ core−shell NPs for MRI, IR thermal imaging, and photothermal therapy.[184]

Facile loading of drugs or biomolecules and their controllable and targeted release based on plasmonic properties enable PENs to be used as remote-controlled delivery carriers for a variety of therapeutic applications. Easy surface modification led to the development of various methods for loading cargo molecules onto PEN carriers, including direct covalent bonds (gold−sulfur bond, gold−nitrogen bond, and thermo-cleavable linker) and non-covalent bonds (oligonucleotide hybridization, hydrogen bonding, electrostatic interaction, and van der Waals interaction). The various drug-loading techniques have been discussed in detail previously.[185,186] After tumor targeting with PENs by passive or active targeting, drugs can be released through the photothermal properties of PEN carriers in a spatial and temporal manner using a synergetic stimuli-responsive design for the efficient delivery of therapeutic agents. This active control of drug release enhances the chemotherapy efficacy and minimizes drug leakage that may kill healthy cells. Some recent examples of PEN-mediated delivery of cargo molecules are shown in Figure 6B. Core−satellite PENs composed of Au/Ag NRs as core and small AuNPs as satellites have been used as nuclear-uptake delivery systems; upon laser irradiation, small drug-loaded Au satellites were detached from the core NR and efficiently accumulated in the nuclei to effectively kill the cancer cells (Figure 6B-i).[187] Vesicular nanostructures composed of ultra-small AuNRs and rGO, loaded with DOX molecules, have been used for laser-induced delivery of DOX to the nucleus.[188] NIR photothermal heating induces DOX release from the vesicular cavity after disassembly of the vesicle, and an intracellular acidic environment induces DOX release from the rGO surface (Figure 6B-ii). Liu et al. reported carbon−silica nanocapsules with gold NPs in the cavity (Au@CSN) for synergistic photothermal and chemotherapy of cancer.[189] Trisoctahedral core−shell Fe_3O_4@Au NPs encapsulated with silica cores have been used for NIR light-controlled release of drug molecules to the tumor site in mice.[190]

Cellular membrane permeability plays crucial role in molecular transport processes, and the non-destructive control of pores in the cellular membrane allows for efficient delivery of therapeutic molecules. In a report by Delcea et al., assembly of AuNPs was used for laser-induced opto-nanoporation in red blood cells, which allows for the diffusion and release of small and large molecules across the membrane.[191] Recently, Meunier et al. reported AuNSs for efficient ultrafast laser-based nanoscale bubble generation and cell membrane perforation, which can be useful for the development of effective gene therapy treatments.[192]

The use of PENs as multimodal theranostic nanoprobes enabling imaging-guided therapy has gained increasing attention. As discussed above, PEN exhibits various useful properties for bioimaging and therapy, allowing multimodal features in one structure with a rational design. Multimodal therapy using PTT/PDT/chemotherapy can increase the therapeutic efficiency, and multimodal imaging can complement finding the precise target location with high spatial resolution. Chen et al. recently reported self-assembled carbon nanotube rings coated with AuNPs for theranostic applications with SERS and PA-based imaging and photothermal effect-based cancer therapy in tumor xenograft mouse models.[193] Zhang et al. designed magnetic gold nanoflowers for MR/PA/SERS-based imaging and PTT-mediated cancer treatment in mice (Figure 6C-i).[194] Flower-like rough structural features are responsible for SERS, PA effect, and photothermal effect; the magnetic core enables real-time MRI. In an another recent report, AuNR and upconversion core−satellite PENs conjugated with the photosensitizer Ce6 were reported as multifunctional theranostic agents for PA/CT/

DOI: 10.1021/jacs.6b09451
J. Am. Chem. Soc. 2016, 138, 14509−14525

MR/UCL-based imaging and PTT/PDT-based combination therapy (Figure 6C-ii).[90] The development of such multifunctional theranostic composite nanoprobes is needed to overcome the limitations of existing cancer therapeutic methods.

6. CONCLUDING REMARKS AND PERSPECTIVES

We have presented brief snapshots of the tremendous growth in the emerging applications of engineered plasmonic nanoprobes in different sectors of biomedical science and engineering. We discussed how contemporary designs of PENs address the challenges of conventional methods and have helped revolutionize the fields of fundamental biotechnologies, biosensing, bioimaging, therapy, and theranostics. Designing, synthesizing, and controlling plasmonic nanostructures on the nanometer scale over a large number of particles and applying the right surface and conjugation chemistries to nanoprobes for a specific application are keys to successful biomedical applications of PENs. Plasmonic nanostructures with well-controlled optical properties led to the development of highly sensitive plasmonic sensors and naked eye detection of biological targets via the aggregation of a large number of plasmonic probes. Tools such as DNA origami and related well-defined organic templates or connectors led to precisely controlled plasmonic nanostructures exhibiting new and augmented plasmonic properties. Particularly, SERS-based biosensing has achieved single-molecule sensitivity and signal reproducibility with hot-spot engineering at nanometer precision and has been used to generate highly enhanced electromagnetic fields in discrete plasmonic assemblies. However, the wide application of SERS in bioimaging remains limited by low tissue penetration of operating light, relatively poor signal reproducibility and quantification of targets, and compatibility and stability of sophisticated SERS tags with complex biological systems. Large light-scattering cross sections and concentration of light in a nanometer volume make PENs ideal for dark-field microscopy; tagging biomolecules with such bright plasmonic rulers can be used for probing crucial biomolecular interactions and measuring small biological distances. The field of chiroplasmonics is emerging with for the study of secondary and tertiary structures of nucleic acids and proteins at the single-molecule level and for the sensitive detection and discrimination of enantiomeric biomolecules, which is challenging using conventional CD spectroscopy. However, new high-yielding methods should be developed to construct chiral plasmonic nanostructures and metamaterials with desired handedness. Plasmon-mediated modulation of fluorescence is also an exciting phenomenon for a numerous molecular detection applications. Fluorescence quenching by the PEN surface has been used as a biodetection switch for a variety of biosensing applications. MEF can be useful for enhancing the application scope and efficiency of conventional fluorophores. Precise tuning of the distance between the fluorophore and metal surface with nanometer precision is challenging for such applications, and more advanced synthetic approaches should be developed.

It should be always noticed that the effect of complex interactions of constituents present in biological media with the PEN surface on the plasmonic properties should be systematically evaluated and controlled, especially for *in vivo* applications, and new bioconjugation strategies for reliably tagging PENs with biomolecules should be developed differently for each specific application under different environments that fit for each application. PENs are ideal platforms for multimodal bioimaging applications because of the access of a variety of plasmon-induced properties of PENs, such as SERS, PA effect, and ease of hybridization with other modalities such PET, CT, and fluorescence. Recent progress in the field of PEN-based therapeutic applications has demonstrated the potential of using PENs for cancer therapy and gene therapy. Combination approaches such as PTT−PDT have shown impressive results in animal models. It was recently shown that the second NIR window (NIR-II; wavelength range: 1000−1400 nm) has several advantages over conventional NIR-I region (750−900 nm) because of reduced photon-scattering probability, deeper tissue penetration, and lower autofluorescence background. Carbon nanotubes,[195] Ag_2S QDs,[196] and organic dyes[197] have already been explored for NIR-II-based bioimaging applications. Au−Cu_9S_5 hybrid NPs were used for photothermal therapy in the NIR-II window.[198] Multifunctional PENs, which can absorb and emit light in the NIR-II region, would certainly be excellent candidates in future diagnostic and therapeutic applications. To extend the scope and find other advantageous properties of PENs, wider and different therapeutic applications should be explored, which would require new design strategies and knowledge of the corresponding nano-biochemistries. Studies of the pharmacological effects, fate after therapy, biodistribution, biodegradation, and excretion from the body should be conducted for the clinical application of PENs. Although most PENs are currently in the initial stages of biomedical applications, a bright future regarding their biomedical applications is anticipated, as suggested by recent examples discussed in this Perspective.

AUTHOR INFORMATION

Corresponding Author

*jmnam@snu.ac.kr

Notes

The authors declare no competing financial interest.

ACKNOWLEDGMENTS

J.-M.N. was supported by a National Research Foundation of Korea (NRF) grant funded by the Korea government (Ministry of Science, ICT & Future Planning (MSIP)) (No. 2016R1A2A1A05005430) and BioNano Health-Guard Research Center funded by the MSIP of Korea as a Global Frontier Project (H-GUARD_2013M3A6B2078947). This research was also supported by the Pioneer Research Center Program through the National Research Foundation of Korea funded by the MSIP (NRF-2012-0009586).

REFERENCES

(1) Halas, N. J.; Lal, S.; Chang, W.-S.; Link, S.; Nordlander, P. *Chem. Rev.* **2011**, *111*, 3913−3961.
(2) Kauranen, M.; Zayats, A. V. *Nat. Photonics* **2012**, *6*, 737−748.
(3) Wang, H.; Kundu, J.; Halas, N. J. *Angew. Chem., Int. Ed.* **2007**, *46*, 9040−9044.
(4) Atwater, H. A.; Polman, A. *Nat. Mater.* **2010**, *9*, 205−213.
(5) Luk'yanchuk, B.; Zheludev, N. I.; Maier, S. A.; Halas, N. J.; Nordlander, P.; Giessen, H.; Chong, C. T. *Nat. Mater.* **2010**, *9*, 707−715.
(6) Herzog, J. B.; Knight, M. W.; Natelson, D. *Nano Lett.* **2014**, *14* (2), 499−503.
(7) Christopher, P.; Xin, H.; Linic, S. *Nat. Chem.* **2011**, *3*, 467−472.
(8) Brongersma, M. L.; Halas, N. J.; Nordlander, P. *Nat. Nanotechnol.* **2015**, *10*, 25−34.
(9) Howes, P. D.; Rana, S.; Stevens, M. M. *Chem. Soc. Rev.* **2014**, *43*, 3835−3853.

DOI: 10.1021/jacs.6b09451
J. Am. Chem. Soc. 2016, 138, 14509−14525

(10) Zhou, W.; Gao, X.; Liu, D.; Chen, X. *Chem. Rev.* **2015**, *115*, 10575−10636.
(11) Tan, S. J.; Campolongo, M. J.; Luo, D.; Cheng, W. *Nat. Nanotechnol.* **2011**, *6* (5), 268−276.
(12) Zhang, N.; Liu, Y. J.; Yang, J.; Su, X.; Deng, J.; Chum, C. C.; Hong, M.; Teng, J. *Nanoscale* **2014**, *6*, 1416−1422.
(13) Jones, M. R.; Osberg, K. D.; MacFarlane, R. J.; Langille, M. R.; Mirkin, C. A. *Chem. Rev.* **2011**, *111*, 3736−3827.
(14) Hao, F.; Sonnefraud, Y.; Van Dorpe, P.; Maier, S. A.; Halas, N. J.; Nordlander, P. *Nano Lett.* **2008**, *8*, 3983−3988.
(15) Langille, M. R.; Personick, M. L.; Zhang, J.; Mirkin, C. A. *J. Am. Chem. Soc.* **2012**, *134*, 14542−14554.
(16) Personick, M. L.; Mirkin, C. A. *J. Am. Chem. Soc.* **2013**, *135*, 18238−18247.
(17) Wang, Y.; Xu, J.; Wang, Y.; Chen, H. *Chem. Soc. Rev.* **2013**, *42*, 2930−2962.
(18) Wang, X.; Tang, Z. *Small* **2016**, DOI: 10.1002/smll.201601115.
(19) Tullius, R.; Karimullah, A. S.; Rodier, M.; Fitzpatrick, B.; Gadegaard, N.; Barron, L. D.; Rotello, V. M.; Cooke, G.; Lapthorn, A.; Kadodwala, M. *J. Am. Chem. Soc.* **2015**, *137*, 8380−8383.
(20) Chen, G.; Roy, I.; Yang, C.; Prasad, P. N. *Chem. Rev.* **2016**, *116*, 2826−2885.
(21) Heath, J. R. *Proc. Natl. Acad. Sci. U. S. A.* **2015**, *112*, 14436−14443.
(22) Kelly, K. L.; Coronado, E.; Zhao, L.; Schatz, G. C. *J. Phys. Chem. B* **2003**, *107*, 668−677.
(23) Liz-Marzán, L. M. *Langmuir* **2006**, *22*, 32−41.
(24) Bohren, C. F.; Huffman, D. R. *Absorption and scattering of light by small particles*; Wiley-Interscience: New York, 1983.
(25) Kreibig, U.; Vollmer, M. *Optical Properties of Metal Clusters*; Springer Verlag: Berlin/Heidelberg, 1995; Vol. *118*.
(26) Link, S.; El-Sayed, M. A. *J. Phys. Chem. B* **1999**, *103*, 4212−4217.
(27) Wang, H.; Brandl, D. W.; Nordlander, P.; Halas, N. J. *Acc. Chem. Res.* **2007**, *40*, 53−62.
(28) Wiley, B. J.; Im, S. H.; Li, Z. Y.; McLellan, J.; Siekkinen, A.; Xia, Y. *J. Phys. Chem. B* **2006**, *110*, 15666−15675.
(29) Xu, X.-B.; Yi, Z.; Li, X.-B.; Wang, Y.-Y.; Geng, X.; Luo, J.-S.; Luo, B.-C.; Yi, Y.-G.; Tang, Y.-J. *J. Phys. Chem. C* **2012**, *116*, 24046−24053.
(30) Waterman, P. C. *Proc. IEEE* **1965**, *53*, 805−812.
(31) Pernice, W. H. P. *J. Comput. Theor. Nanosci.* **2010**, *7*, 1−14.
(32) Chen, Y.; Nielsen, T. R.; Gregersen, N.; Lodahl, P.; Mørk. *Phys. Rev. B: Condens. Matter Mater. Phys.* **2010**, *81*, 125431.
(33) Liaw, J.-W. *J. Opt. Soc. Am. A* **2006**, *23*, 108−16.
(34) Park, K.; Biswas, S.; Kanel, S.; Nepal, D.; Vaia, R. A. *J. Phys. Chem. C* **2014**, *118*, 5918−5926.
(35) Brinson, B. E.; Lassiter, J. B.; Levin, C. S.; Bardhan, R.; Mirin, N.; Halas, N. J. *Langmuir* **2008**, *24*, 14166−14171.
(36) Skrabalak, S. E.; Chen, J.; Sun, Y.; Lu, X.; Au, L.; Cobley, C. M.; Xia, Y. *Acc. Chem. Res.* **2008**, *41*, 1587−1595.
(37) Liu, X.-L.; Wang, J.-H.; Liang, S.; Yang, D.-J.; Nan, F.; Ding, S.-J.; Zhou, L.; Hao, Z.-H.; Wang, Q.-Q. *J. Phys. Chem. C* **2014**, *118*, 9659−9664.
(38) Klinkova, A.; Choueiri, R. M.; Kumacheva, E. *Chem. Soc. Rev.* **2014**, *43*, 3976−3991.
(39) Su, K. H.; Wei, Q. H.; Zhang, X.; Mock, J. J.; Smith, D. R.; Schultz, S. *Nano Lett.* **2003**, *3*, 1087−1090.
(40) Jain, P. K.; Huang, W.; El-Sayed, M. A. *Nano Lett.* **2007**, *7*, 2080−2088.
(41) Lim, D.-K.; Jeon, K.-S.; Kim, H. M.; Nam, J.-M.; Suh, Y. D. *Nat. Mater.* **2010**, *9*, 60−67.
(42) Haidar, I.; Aubard, J.; Levi, G.; Lau-Truong, S.; Mouton, L.; Neuville, D. R.; Felidj, N.; Boubekeur-Lecaque, L. *J. Phys. Chem. C* **2015**, *119*, 23149−23158.
(43) Sönnichsen, C.; Reinhard, B. M.; Liphardt, J.; Alivisatos, P. *Nat. Biotechnol.* **2005**, *23*, 741−745.
(44) Chen, G.; Wang, Y.; Tan, L. H.; Yang, M.; Tan, L. S.; Chen, Y.; Chen, H. *J. Am. Chem. Soc.* **2009**, *131*, 4218−4219.
(45) Li, J. F.; Huang, Y. F.; Ding, Y.; Yang, Z. L.; Li, S. B.; Zhou, X. S.; Fan, F. R.; Zhang, W.; Zhou, Z. Y.; Wu, D. Y.; Ren, B.; Wang, Z. L.; Tian, Z. Q. *Nature* **2010**, *464*, 392−395.
(46) Mertens, J.; Eiden, A. L.; Sigle, D. O.; Huang, F.; Lombardo, A.; Sun, Z.; Sundaram, R. S.; Colli, A.; Tserkezis, C.; Aizpurua, J.; Milana, S.; Ferrari, A. C.; Baumberg, J. J. *Nano Lett.* **2013**, *13*, 5033−5038.
(47) Prodan, E.; Nordlander, P. *J. Chem. Phys.* **2004**, *120*, 5444−5454.
(48) Jain, P. K.; El-Sayed, M. A. *Chem. Phys. Lett.* **2010**, *487*, 153−164.
(49) Fan, J. a; Wu, C.; Bao, K.; Bao, J.; Bardhan, R.; Halas, N. J.; Manoharan, V. N.; Nordlander, P.; Shvets, G.; Capasso, F. *Science* **2010**, *328*, 1135−1138.
(50) Tomalia, D. A.; Khanna, S. N. *Chem. Rev.* **2016**, *116*, 2705−2774.
(51) Grzelczak, M.; Vermant, J.; Furst, E. M.; Liz-Marzán, L. M. *ACS Nano* **2010**, *4*, 3591−3605.
(52) Xu, X.; Rosi, N. L.; Wang, Y.; Huo, F.; Mirkin, C. A. *J. Am. Chem. Soc.* **2006**, *128*, 9286−9287.
(53) Cutler, J. I.; Auyeung, E.; Mirkin, C. A. *J. Am. Chem. Soc.* **2012**, *134*, 1376−1391.
(54) Kumar, A.; Hwang, J.-H.; Kumar, S.; Nam, J.-M. *Chem. Commun.* **2013**, *49*, 2597−2609.
(55) Chao, J.; Lin, Y.; Liu, H.; Wang, L.; Fan, C. *Mater. Today* **2015**, *18*, 326−335.
(56) Wang, Z.; Zhang, J.; Ekman, J. M.; Kenis, P. J. A.; Lu, Y. *Nano Lett.* **2010**, *10*, 1886−1891.
(57) Song, T.; Tang, L.; Tan, L. H.; Wang, X.; Satyavolu, N. S. R.; Xing, H.; Wang, Z.; Li, J.; Liang, H.; Lu, Y. *Angew. Chem., Int. Ed.* **2015**, *54*, 8114−8118.
(58) Tan, L. H.; Yue, Y.; Satyavolu, N. S. R.; Ali, A. S.; Wang, Z.; Wu, Y.; Lu, Y. *J. Am. Chem. Soc.* **2015**, *137*, 14456−14464.
(59) Oh, J.-W.; Lim, D.-K.; Kim, G.-H.; Suh, Y. D.; Nam, J.-M. *J. Am. Chem. Soc.* **2014**, *136*, 14052−14059.
(60) Lee, J.-H.; Kim, G.-H.; Nam, J.-M. *J. Am. Chem. Soc.* **2012**, *134*, 5456−5459.
(61) Sun, W.; Boulais, E.; Hakobyan, Y.; Wang, W. L.; Guan, A.; Bathe, M.; Yin, P. *Science* **2014**, *346*, 1258361.
(62) Jones, M. R.; Seeman, N. C.; Mirkin, C. A. *Science* **2015**, *347*, 6224.
(63) Seeman, N. C. *Nature* **2003**, *421*, 427−431.
(64) Rothemund, P. W. K. *Nature* **2006**, *440*, 297−302.
(65) Zhang, Y.; Chao, J.; Liu, H.; Wang, F.; Su, S.; Liu, B.; Zhang, L.; Shi, J.; Wang, L.; Huang, W.; Wang, L.; Fan, C. *Angew. Chem., Int. Ed.* **2016**, *55*, 8036−8040.
(66) Lan, X.; Lu, X.; Shen, C.; Ke, Y.; Ni, W.; Wang, Q. *J. Am. Chem. Soc.* **2015**, *137*, 457−462.
(67) Urban, M. J.; Dutta, P. K.; Wang, P.; Duan, X.; Shen, X.; Ding, B.; Ke, Y.; Liu, N. *J. Am. Chem. Soc.* **2016**, *138*, 5495−5498.
(68) Zhou, C.; Duan, X.; Liu, N. *Nat. Commun.* **2015**, *6*, 8102.
(69) Urban, M. J.; Zhou, C.; Duan, X.; Liu, N. *Nano Lett.* **2015**, *15*, 8392−8396.
(70) Sefah, K.; Shangguan, D.; Xiong, X.; O'Donoghue, M. B.; Tan, W. *Nat. Protoc.* **2010**, *5*, 1169−1185.
(71) Tan, Y. N.; Lee, J. Y.; Wang, D. I. C. *J. Am. Chem. Soc.* **2010**, *132*, 5677−5686.
(72) Slocik, J. M.; Moore, J. T.; Wright, D. W. *Nano Lett.* **2002**, *2*, 169−173.
(73) Naik, R. R.; Jones, S. E.; Murray, C. J.; McAuliffe, J. C.; Vaia, R. A.; Stone, M. O. *Adv. Funct. Mater.* **2004**, *14*, 25−30.
(74) Naik, R. R.; Stringer, S. J.; Agarwal, G.; Jones, S. E.; Stone, M. O. *Nat. Mater.* **2002**, *1*, 169−172.
(75) Djalali, R.; Chen, Y. F.; Matsui, H. *J. Am. Chem. Soc.* **2003**, *125*, 5873−5879.
(76) Chen, C. L.; Zhang, P.; Rosi, N. L. *J. Am. Chem. Soc.* **2008**, *130*, 13555−13557.
(77) Slocik, J. M.; Govorov, A. O.; Naik, R. R. *Nano Lett.* **2011**, *11*, 701−705.
(78) Briggs, B. D.; Knecht, M. R. *J. Phys. Chem. Lett.* **2012**, *3*, 405−418.
(79) Anker, J. N.; Hall, W. P.; Lyandres, O.; Shah, N. C.; Zhao, J.; Van Duyne, R. P. *Nat. Mater.* **2008**, *7*, 442−453.
(80) Wang, Y.; Yan, B.; Chen, L. *Chem. Rev.* **2013**, *113*, 1391−1428.
(81) Lee, J.-H.; Nam, J.-M.; Jeon, K.-S.; Lim, D.-K.; Kim, H.; Kwon, S.; Lee, H.; Suh, Y. D. *ACS Nano* **2012**, *6*, 9574−9584.

DOI: 10.1021/jacs.6b09451
J. Am. Chem. Soc. 2016, 138, 14509−14525

(82) Aslan, K.; Gryczynski, I.; Malicka, J.; Matveeva, E.; Lakowicz, J. R.; Geddes, C. D. *Curr. Opin. Biotechnol.* **2005**, *16*, 55−62.
(83) Li, W.; Chen, X. *Nanomedicine (London, U. K.)* **2015**, *10*, 299−320.
(84) Li, C. *Nat. Mater.* **2014**, *13*, 110−115.
(85) Abadeer, N. S.; Murphy, C. J. *J. Phys. Chem. C* **2016**, *120*, 4691−4716.
(86) Gao, L.; Liu, R.; Gao, F.; Wang, Y.; Jiang, X.; Gao, X. *ACS Nano* **2014**, *8*, 7260−7271.
(87) Kumar, A.; Kumar, S.; Rhim, W.-K.; Kim, G.-H.; Nam, J.-M. *J. Am. Chem. Soc.* **2014**, *136*, 16317−16325.
(88) Luo, Y.-L.; Shiao, Y.-S.; Huang, Y.-F. *ACS Nano* **2011**, *5*, 7796−7804.
(89) Raeesi, V.; Chou, L. Y. T.; Chan, W. C. W. *Adv. Mater.* **2016**, *28*, 8511−8518.
(90) Sun, M.; Xu, L.; Ma, W.; Wu, X.; Kuang, H.; Wang, L.; Xu, C. *Adv. Mater.* **2016**, *28*, 898−904.
(91) Walkey, C. D.; Chan, W. C. W. *Chem. Soc. Rev.* **2012**, *41*, 2780−2799.
(92) Zhou, W.; Gao, X.; Liu, D.; Chen, X. *Chem. Rev.* **2015**, *115*, 10575−10636.
(93) Zhang, Y.; Guo, Y.; Xianyu, Y.; Chen, W.; Zhao, Y.; Jiang, X. *Adv. Mater.* **2013**, *25*, 3802−3819.
(94) Mayer, K. M.; Hafner, J. H. *Chem. Rev.* **2011**, *111*, 3828−3857.
(95) Xianyu, Y.; Wang, Z.; Jiang, X. *ACS Nano* **2014**, *8*, 12741−12747.
(96) Qu, W.; Liu, Y.; Liu, D.; Wang, Z.; Jiang, X. *Angew. Chem., Int. Ed.* **2011**, *50*, 3442−3445.
(97) Bui, M. P. N.; Ahmed, S.; Abbas, A. *Nano Lett.* **2015**, *15*, 6239−6246.
(98) Yang, X.; Yu, Y.; Gao, Z. *ACS Nano* **2014**, *8*, 4902−4907.
(99) Rodríguez-Lorenzo, L.; de la Rica, R.; Álvarez-Puebla, R. a.; Liz-Marzán, L. M.; Stevens, M. M. *Nat. Mater.* **2012**, *11*, 604−607.
(100) Joshi, G. K.; Deitz-Mcelyea, S.; Johnson, M.; Mali, S.; Korc, M.; Sardar, R. *Nano Lett.* **2014**, *14*, 6955−6963.
(101) Lee, Y. K.; Kim, S.; Oh, J.-W.; Nam, J.-M. *J. Am. Chem. Soc.* **2014**, *136*, 4081−4088.
(102) Tajon, C. A.; Seo, D.; Asmussen, J.; Shah, N.; Jun, Y. W.; Craik, C. S. *ACS Nano* **2014**, *8*, 9199−9208.
(103) Wang, H.; Rong, G.; Yan, B.; Yang, L.; Reinhard, B. M. *Nano Lett.* **2011**, *11*, 498−504.
(104) Wang, J.; Boriskina, S. V.; Wang, H.; Reinhard, B. M. *ACS Nano* **2011**, *5*, 6619−6628.
(105) Austin, L. a; Kang, B.; Yen, C.; El-sayed, M. A. *J. Am. Chem. Soc.* **2011**, *133*, 17594−17597.
(106) Wang, J.; Yu, X.; Boriskina, S. V.; Reinhard, B. M. *Nano Lett.* **2012**, *12*, 3231−3237.
(107) Fraire, J. C.; Masseroni, L.; Jausoro, I.; Perassi, E. M.; Diaz Añel, A. M.; Coronado, E. A. *ACS Nano* **2014**, *8*, 8942−8958.
(108) Wang, X.; Cui, Y.; Irudayaraj, J. *ACS Nano* **2015**, *9*, 11924−11932.
(109) Lee, S. E.; Chen, Q.; Bhat, R.; Petkiewicz, S.; Smith, J. M.; Ferry, V. E.; Correia, A. L.; Alivisatos, A. P.; Bissell, M. J. *Nano Lett.* **2015**, *15*, 4564−4570.
(110) Lieberman, I.; Shemer, G.; Fried, T.; Kosower, E. M.; Markovich, G. *Angew. Chem., Int. Ed.* **2008**, *47*, 4855−4857.
(111) Govorov, A. O.; Fan, Z.; Hernandez, P.; Slocik, J. M.; Naik, R. R. *Nano Lett.* **2010**, *10*, 1374−1382.
(112) Liu, W.; Zhu, Z.; Deng, K.; Li, Z.; Zhou, Y.; Qiu, H.; Gao, Y.; Che, S.; Tang, Z. *J. Am. Chem. Soc.* **2013**, *135*, 9659−9664.
(113) Wu, X.; Xu, L.; Ma, W.; Liu, L.; Kuang, H.; Yan, W.; Wang, L.; Xu, C. *Adv. Funct. Mater.* **2015**, *25*, 850−854.
(114) Wu, X.; Xu, L.; Liu, L.; Ma, W.; Yin, H.; Kuang, H.; Wang, L.; Xu, C.; Kotov, N. A. *J. Am. Chem. Soc.* **2013**, *135*, 18629−18636.
(115) Zhao, Y.; Xu, L.; Ma, W.; Wang, L.; Kuang, H.; Xu, C.; Kotov, N. A. *Nano Lett.* **2014**, *14*, 3908−3913.
(116) Wu, X.; Xu, L.; Ma, W.; Liu, L.; Kuang, H.; Kotov, N. A.; Xu, C. *Adv. Mater.* **2016**, *28*, 5907−5915.
(117) Li, S.; Xu, L.; Ma, W.; Wu, X.; Sun, M.; Kuang, H.; Wang, L.; Kotov, N. A.; Xu, C. *J. Am. Chem. Soc.* **2016**, *138* (1), 306−312.
(118) Valev, V. K.; Baumberg, J. J.; Sibilia, C.; Verbiest, T. *Adv. Mater.* **2013**, *25* (18), 2517−2534.
(119) Hendry, E.; Carpy, T.; Johnston, J.; Popland, M.; Mikhaylovskiy, R. V.; Lapthorn, A. J.; Kelly, S. M.; Barron, L. D.; Gadegaard, N.; Kadodwala, M. *Nat. Nanotechnol.* **2010**, *5*, 783−787.
(120) Tullius, R.; Karimullah, A. S.; Rodier, M.; Fitzpatrick, B.; Gadegaard, N.; Barron, L. D.; Rotello, V. M.; Cooke, G.; Lapthorn, A.; Kadodwala, M. *J. Am. Chem. Soc.* **2015**, *137*, 8380−8383.
(121) Wang, Y.; Yan, B.; Chen, L. *Chem. Rev.* **2013**, *113*, 1391−1428.
(122) Lane, L. A.; Qian, X.; Nie, S. *Chem. Rev.* **2015**, *115*, 10489−10529.
(123) Nie, S.; Emory, S. R. *Science* **1997**, *275*, 1102−1106.
(124) Cao, Y. C.; Jin, R.; Mirkin, C. a. *Science* **2002**, *297*, 1536−1540.
(125) Lim, D.-K.; Jeon, K.-S.; Hwang, J.-H.; Kim, H.; Kwon, S.; Suh, Y. D.; Nam, J.-M. *Nat. Nanotechnol.* **2011**, *6*, 452−460.
(126) Lee, H.; Lee, J.-H.; Jin, S. M.; Suh, Y. D.; Nam, J.-M. *Nano Lett.* **2013**, *13*, 6113−6121.
(127) Lee, H.; Kim, G.-H.; Lee, J.-H.; Kim, N. H.; Nam, J.-M.; Suh, Y. D. *Nano Lett.* **2015**, *15*, 4628−4636.
(128) Lee, J.-H.; You, M.-H.; Kim, G.-H.; Nam, J.-M. *Nano Lett.* **2014**, *14*, 6217−6225.
(129) Xu, L.; Yan, W.; Ma, W.; Kuang, H.; Wu, X.; Liu, L.; Zhao, Y.; Wang, L.; Xu, C. *Adv. Mater.* **2015**, *27*, 1706−1711.
(130) La Rocca, R.; Messina, G. C.; Dipalo, M.; Shalabaeva, V.; De Angelis, F. *Small* **2015**, *11*, 4632−4637.
(131) Lu, G.; De Keersmaecker, H.; Su, L.; Kenens, B.; Rocha, S.; Fron, E.; Chen, C.; Van Dorpe, P.; Mizuno, H.; Hofkens, J.; Hutchison, J. A.; Uji-I, H. *Adv. Mater.* **2014**, *26* (30), 5124−5128.
(132) Niu, J. J.; Schrlau, M. G.; Friedman, G.; Gogotsi, Y. *Small* **2011**, *7*, 540−545.
(133) Lussier, F.; Brulé, T.; Vishwakarma, M.; Das, T.; Spatz, J. P.; Masson, J.-F. *Nano Lett.* **2016**, *16*, 3866−3871.
(134) Ling, X.; Xie, L.; Fang, Y.; Xu, H.; Zhang, H.; Kong, J.; Dresselhaus, M. S.; Zhang, J.; Liu, Z. *Nano Lett.* **2010**, *10*, 553−561.
(135) Yi, N.; Zhang, C.; Song, Q.; Xiao, S. *Sci. Rep.* **2016**, *6*, 25134.
(136) Bian, X.; Song, Z.-L.; Qian, Y.; Gao, W.; Cheng, Z.-Q.; Chen, L.; Liang, H.; Ding, D.; Nie, X.-K.; Chen, Z.; Tan, W. *Sci. Rep.* **2014**, *4*, 6093.
(137) Lai, X.-F.; Zou, Y.-X.; Wang, S.-S.; Zheng, M.-J.; Hu, X.-X.; Liang, H.; Xu, Y.-T.; Wang, X.-W.; Ding, D.; Chen, L.; Chen, Z.; Tan, W. *Anal. Chem.* **2016**, *88*, 5385−5391.
(138) Duan, B.; Zhou, J.; Fang, Z.; Wang, C.; Wang, X.; Hemond, H. F.; Chan-Park, M.; Duan, H. *Nanoscale* **2015**, *7*, 12606−12613.
(139) Xu, W.; Ling, X.; Xiao, J.; Dresselhaus, M. S.; Kong, J.; Xu, H.; Liu, Z.; Zhang, J. *Proc. Natl. Acad. Sci. U. S. A.* **2012**, *109*, 9281−9286.
(140) Wang, P.; Liang, O.; Zhang, W.; Schroeder, T.; Xie, Y. H. *Adv. Mater.* **2013**, *25*, 4918−4924.
(141) Wang, P.; Xia, M.; Liang, O.; Sun, K.; Cipriano, A. F.; Schroeder, T.; Liu, H.; Xie, Y. H. *Anal. Chem.* **2015**, *87*, 10255−10261.
(142) Stöckle, R. M.; Suh, Y. D.; Deckert, V.; Zenobi, R. *Chem. Phys. Lett.* **2000**, *318*, 131−136.
(143) Taguchi, A.; Yu, J.; Verma, P.; Kawata, S. *Nanoscale* **2015**, *7*, 17424−17433.
(144) Rusciano, G.; Zito, G.; Isticato, R.; Sirec, T.; Ricca, E.; Bailo, E.; Sasso, A. *ACS Nano* **2014**, *8*, 12300−12309.
(145) Wood, B. R.; Bailo, E.; Khiavi, M. A.; Tilley, L.; Deed, S.; Deckert-Gaudig, T.; Mcnaughton, D.; Deckert, V. *Nano Lett.* **2011**, *11*, 1868−1873.
(146) Wood, B. R.; Asghari-Khiavi, M.; Bailo, E.; McNaughton, D.; Deckert, V. *Nano Lett.* **2012**, *12*, 1555−1560.
(147) Yorulmaz, M.; Khatua, S.; Zijlstra, P.; Gaiduk, A.; Orrit, M. *Nano Lett.* **2012**, *12*, 4385−4391.
(148) Rao, W.; Li, Q.; Wang, Y.; Li, T.; Wu, L. *ACS Nano* **2015**, *9*, 2783−2791.
(149) Wu, X.; Ming, T.; Wang, X.; Wang, P.; Wang, J.; Chen, J. *ACS Nano* **2010**, *4*, 113−120.
(150) Yun, C. S.; Javier, A.; Jennings, T.; Fisher, M.; Hira, S.; Peterson, S.; Hopkins, B.; Reich, N. O.; Strouse, G. F. *J. Am. Chem. Soc.* **2005**, *127*, 3115−3119.

DOI: 10.1021/jacs.6b09451
J. Am. Chem. Soc. 2016, 138, 14509−14525

(151) Breshike, C. J.; Riskowski, R. A.; Strouse, G. F. *J. Phys. Chem. C* **2013**, *117*, 23942−23949.
(152) Choi, C. K. K.; Li, J.; Wei, K.; Xu, Y. J.; Ho, L. W. C.; Zhu, M.; To, K. K. W.; Choi, C. H. J.; Bian, L. *J. Am. Chem. Soc.* **2015**, *137*, 7337−7346.
(153) Liu, D.; Wang, S.; Swierczewska, M.; Huang, X.; Bhirde, A. A.; Sun, J.; Wang, Z.; Yang, M.; Jiang, X.; Chen, X. *ACS Nano* **2012**, *6*, 10999−11008.
(154) Bardhan, R.; Grady, N. K.; Halas, N. J. *Small* **2008**, *4*, 1716−1722.
(155) Bardhan, R.; Grady, N. K.; Cole, J. R.; Joshi, A.; Halas, N. J. *ACS Nano* **2009**, *3*, 744−752.
(156) Tam, F.; Goodrich, G. P.; Johnson, B. R.; Halas, N. J. *Nano Lett.* **2007**, *7*, 496−501.
(157) Khatua, S.; Paulo, P. M. R.; Yuan, H.; Gupta, A.; Zijlstra, P.; Orrit, M. *ACS Nano* **2014**, *8*, 4440−4449.
(158) Ayala-Orozco, C.; Liu, J. G.; Knight, M. W.; Wang, Y.; Day, J. K.; Nordlander, P.; Halas, N. J. *Nano Lett.* **2014**, *14*, 2926−2933.
(159) Camposeo, A.; Persano, L.; Manco, R.; Wang, Y.; Del Carro, P.; Zhang, C.; Li, Z. Y.; Pisignano, D.; Xia, Y. *ACS Nano* **2015**, *9*, 10047−10054.
(160) Zhang, B.; Kumar, R. B.; Dai, H.; Feldman, B. J. *Nat. Med.* **2014**, *20*, 948−953.
(161) Koh, B.; Li, X.; Zhang, B.; Yuan, B.; Lin, Y.; Antaris, A. L.; Wan, H.; Gong, M.; Yang, J.; Zhang, X.; Liang, Y.; Dai, H. *Small* **2016**, *12*, 457−465.
(162) Samanta, A.; Zhou, Y.; Zou, S.; Yan, H.; Liu, Y. *Nano Lett.* **2014**, *14*, 5052−5057.
(163) Ji, B.; Giovanelli, E.; Habert, B.; Spinicelli, P.; Nasilowski, M.; Xu, X.; Lequeux, N.; Hugonin, J.-P.; Marquier, F.; Greffet, J.-J.; Dubertret, B. *Nat. Nanotechnol.* **2015**, *10*, 170−175.
(164) Guarrotxena, N.; Bazan, G. C. *Adv. Mater.* **2014**, *26*, 1941−1946.
(165) Kim, Y.-H.; Jeon, J.; Hong, S. H.; Rhim, W.-K.; Lee, Y.-S.; Youn, H.; Chung, J.-K.; Lee, M. C.; Lee, D. S.; Kang, K. W.; Nam, J.-M. *Small* **2011**, *7*, 2052.
(166) Kang, J. W.; So, P. T. C.; Dasari, R. R.; Lim, D. K. *Nano Lett.* **2015**, *15*, 1766−1772.
(167) Bohndiek, S. E.; Wagadarikar, A.; Zavaleta, C. L.; Van de Sompel, D.; Garai, E.; Jokerst, J. V.; Yazdanfar, S.; Gambhir, S. S. *Proc. Natl. Acad. Sci. U. S. A.* **2013**, *110*, 12408−12413.
(168) Cheng, K.; Kothapalli, S. R.; Liu, H.; Koh, A. L.; Jokerst, J. V.; Jiang, H.; Yang, M.; Li, J.; Levi, J.; Wu, J. C.; Gambhir, S. S.; Cheng, Z. *J. Am. Chem. Soc.* **2014**, *136*, 3560−3571.
(169) Deng, H.; Dai, F.; Ma, G.; Zhang, X. *Adv. Mater.* **2015**, *27*, 3645−3653.
(170) Von Maltzahn, G.; Park, J. H.; Agrawal, A.; Bandaru, N. K.; Das, S. K.; Sailor, M. J.; Bhatia, S. N. *Cancer Res.* **2009**, *69*, 3892−3900.
(171) Melancon, M. P.; Lu, W.; Yang, Z.; Zhang, R.; Cheng, Z.; Elliot, A. M.; Stafford, J.; Olson, T.; Zhang, J. Z.; Li, C. *Mol. Cancer Ther.* **2008**, *7*, 1730−1739.
(172) Bardhan, R.; Lal, S.; Joshi, A.; Halas, N. J. *Acc. Chem. Res.* **2011**, *44*, 936−946.
(173) Skrabalak, S. E.; Chen, J.; Sun, Y.; Lu, X.; Au, L.; Cobley, C. M.; Xia, Y. *Acc. Chem. Res.* **2008**, *41*, 1587−1595.
(174) Chen, J.; Glaus, C.; Laforest, R.; Zhang, Q.; Yang, M.; Gidding, M.; Welch, M. J.; Xia, Y. *Small* **2010**, *6*, 811−817.
(175) Hirsch, L. R.; Gobin, A. M.; Lowery, A. R.; Tam, F.; Drezek, R. A.; Halas, N. J.; West, J. L. *Ann. Biomed. Eng.* **2006**, *34*, 15−22.
(176) Chen, J.; Wiley, B.; Li, Z. Y.; Campbell, D.; Saeki, F.; Cang, H.; Au, L.; Lee, J.; Li, X.; Xia, Y. *Adv. Mater.* **2005**, *17*, 2255−2261.
(177) Yuan, H.; Fales, A. M.; Vo-Dinh, T. *J. Am. Chem. Soc.* **2012**, *134*, 11358−11361.
(178) Wang, S.; Huang, P.; Nie, L.; Xing, R.; Liu, D.; Wang, Z.; Lin, J.; Chen, S.; Niu, G.; Lu, G.; Chen, X. *Adv. Mater.* **2013**, *25*, 3055−3061.
(179) Qiu, X.; Liu, X.; Zhang, W.; Zhang, H.; Jiang, T.; Fan, D.; Luo, Y. *Anal. Chem.* **2015**, *87*, 6303−6310.
(180) Han, J.; Li, J.; Jia, W.; Yao, L.; Li, X.; Jiang, L.; Tian, Y. *Int. J. Nanomed.* **2014**, *9*, 517−526.
(181) Vijayaraghavan, P.; Liu, C. H.; Vankayala, R.; Chiang, C. S.; Hwang, K. C. *Adv. Mater.* **2014**, *26*, 6689−6695.
(182) Ayala-Orozco, C.; Urban, C.; Knight, M. W.; Urban, A. S.; Neumann, O.; Bishnoi, S. W.; Mukherjee, S.; Goodman, A. M.; Charron, H.; Mitchell, T.; Shea, M.; Roy, R.; Nanda, S.; Schiff, R.; Halas, N. J.; Joshi, A. *ACS Nano* **2014**, *8*, 6372−6381.
(183) Hu, Y.; Yang, Y.; Wang, H.; Du, H. *ACS Nano* **2015**, *9*, 8744−8754.
(184) Tian, Q.; Hu, J.; Zhu, Y.; Zou, R.; Chen, Z.; Yang, S.; Li, R.; Su, Q.; Han, Y.; Liu, X. *J. Am. Chem. Soc.* **2013**, *135*, 8571−8577.
(185) Dreaden, E. C.; Alkilany, A. M.; Huang, X.; Murphy, C. J.; El-Sayed, M. a. *Chem. Soc. Rev.* **2012**, *41*, 2740.
(186) Yang, X.; Yang, M.; Pang, B.; Vara, M.; Xia, Y. *Chem. Rev.* **2015**, *115*, 10410−10488.
(187) Qiu, L.; Chen, T.; Öçsoy, I.; Yasun, E.; Wu, C.; Zhu, G.; You, M.; Han, D.; Jiang, J.; Yu, R.; Tan, W. *Nano Lett.* **2015**, *15*, 457−463.
(188) Song, J.; Yang, X.; Jacobson, O.; Lin, L.; Huang, P.; Niu, G.; Ma, Q.; Chen, X. *ACS Nano* **2015**, *9*, 9199−9209.
(189) Li, L.; Chen, C.; Liu, H.; Fu, C.; Tan, L.; Wang, S.; Fu, S.; Liu, X.; Meng, X.; Liu, H. *Adv. Funct. Mater.* **2016**, *26*, 4252−4261.
(190) Li, W. P.; Liao, P. Y.; Su, C. H.; Yeh, C. S. *J. Am. Chem. Soc.* **2014**, *136*, 10062−10075.
(191) Delcea, M.; Sternberg, N.; Yashchenok, A. M.; Georgieva, R.; Bäumler, H.; Möhwald, H.; Skirtach, A. G. *ACS Nano* **2012**, *6* (5), 4169−4180.
(192) Neumann, O.; Neumann, A. D.; Silva, E.; Ayala-Orozco, C.; Tian, S.; Nordlander, P.; Halas, N. J. *Nano Lett.* **2015**, *15*, 7880−7885.
(193) Song, J.; Wang, F.; Yang, X.; Ning, B.; Harp, M. G.; Culp, S. H.; Hu, S.; Huang, P.; Nie, L.; Chen, J.; Chen, X. *J. Am. Chem. Soc.* **2016**, *138*, 7005−7015.
(194) Huang, J.; Guo, M.; Ke, H.; Zong, C.; Ren, B.; Liu, G.; Shen, H.; Ma, Y.; Wang, X.; Zhang, H.; Deng, Z.; Chen, H.; Zhang, Z. *Adv. Mater.* **2015**, *27*, 5049−5056.
(195) Welsher, K.; Liu, Z.; Sherlock, S. P.; Robinson, J. T.; Chen, Z.; Daranciang, D.; Dai, H. *Nat. Nanotechnol.* **2009**, *4*, 773−780.
(196) Hong, G.; Robinson, J. T.; Zhang, Y.; Diao, S.; Antaris, A. L.; Wang, Q.; Dai, H. *Angew. Chem., Int. Ed.* **2012**, *51*, 9818−9821.
(197) Semonin, O. E.; Johnson, J. C.; Luther, J. M.; Midgett, A. G.; Nozik, A. J.; Beard, M. C. *J. Phys. Chem. Lett.* **2010**, *1*, 2445−2450.
(198) Ding, X.; Liow, C. H.; Zhang, M.; Huang, R.; Li, C.; Shen, H.; Liu, M.; Zou, Y.; Gao, N.; Zhang, Z.; Li, Y.; Wang, Q.; Li, S.; Jiang, J. *J. Am. Chem. Soc.* **2014**, *136*, 15684−15693.

DOI: 10.1021/jacs.6b09451
J. Am. Chem. Soc. 2016, 138, 14509−14525